nature structural & molecular biology

Caspase-activated phosphoinositide binding by CNT-1 promotes apoptosis by inhibiting the AKT pathway

Akihisa Nakagawa, Kelly D Sullivan & Ding Xue

Inactivation of cell-survival factors is a crucial step in apoptosis. The phosphoinositide 3-kinase (PI3K)-AKT signaling pathway promotes cell growth, proliferation and survival, and its deregulation causes cancer. How this pathway is suppressed to promote apoptosis is poorly understood. Here we report the identification of a CED-3 caspase substrate in *Caenorhabditis elegans*, CNT-1, that is cleaved during apoptosis to generate an N-terminal phosphoinositide-binding fragment (tCNT-1). tCNT-1 translocates from the cytoplasm to the plasma membrane and blocks AKT binding to phosphatidylinositol (3,4,5)-trisphosphate, thereby disabling AKT activation and its prosurvival activity. Our findings reveal a new mechanism that negatively regulates AKT cell signaling to promote apoptosis and that may restrict cell growth and proliferation in normal cells.

© 2014 Nature America, Inc. All rights reserved.

One major unanswered question in apoptosis, an essential process in animal development and homeostasis, is how the cell-suicide program is executed in a highly coordinated fashion so that the dying cell is disassembled and removed swiftly without causing any deteriorating outcomes[1]. The cell death–execution process is activated by caspases, which are aspartate-specific cysteine proteases that cleave multiple substrates to orchestrate cellular disassembly, including chromosome fragmentation, nuclear-membrane breakdown and phagocytosis of apoptotic cells[1,2]. Numerous caspase substrates have been identified in mammals, and some are involved in cell-death execution *in vivo*[2]. For example, the PAK2 kinase is activated by caspase-3 cleavage, which is required for the fragmentation of dying cells into apoptotic bodies[3]. In *C. elegans*, many apoptosis regulators and executors are conserved[4], including the CED-3 caspase and CED-3 activator CED-4 (homologous to the human caspase activator Apaf-1), both of which are essential for apoptosis in *C. elegans*. How CED-3 kills cells by proteolytic cleavage is poorly understood. Recently, the Dicer RNase (DCR-1) was found to be converted into a DNase upon CED-3 cleavage during apoptosis, to initiate apoptotic chromosome fragmentation[5]. Similarly, CED-3 cleavage of the mitochondrial fission protein DRP-1 and the multipass transmembrane protein CED-8 generates C-terminal cleavage products that promote mitochondria elimination and phosphatidylserine externalization, respectively, in apoptotic cells[6,7]. Thus, CED-3 cleavage of DCR-1, DRP-1 and CED-8 activates three different cell-disassembly events that facilitate cell killing. In this study, we report a new CED-3 substrate, CNT-1, whose cleavage by CED-3 activates an N-terminal cleavage product, truncated CNT-1 (tCNT-1), that promotes apoptosis by suppressing the AKT prosurvival activity.

In mammals, the PI3K-AKT pathway is critical for cell growth, proliferation, survival and metabolism[8,9]. Hyperactivation of this pathway results in cancers, thus revealing the oncogenic potential of PI3K-AKT signaling components[10–12], whereas impaired signaling in this pathway causes diabetes and cardiovascular disease[13,14]. In *C. elegans*, the AKT homologs AKT-1 and AKT-2 act in the insulin and insulin-like growth factor signaling (IIS) pathway to regulate lifespan, development, metabolism and stress resistance[15–17]. In the IIS pathway, the insulin receptor–like protein DAF-2 activates the PI3K complex AGE-1–AAP-1 (refs. 18–20) to lead to the generation of phosphatidylinositol (3,4,5)-trisphosphate (PIP_3) on the inner leaflet of the plasma membrane. PIP_3 may then recruit the serine/threonine kinases PDK-1, AKT-1, AKT-2 and SGK-1 to the plasma membrane by engaging their pleckstrin homology (PH) domains[21–23], as has been shown with mammalian AKT[9]. PDK-1 probably phosphorylates and activates AKT-1, AKT-2 and SGK-1, which negatively regulate the activity of the forkhead transcription factor DAF-16 (refs. 24,25) and prevent its translocation from the cytosol to the nucleus[26,27]. The PI3K-AKT pathway is negatively regulated by the lipid phosphatase DAF-18 (homologous to human phosphatase and tensin homolog, PTEN), which dephosphorylates and converts PIP_3 to phosphatidylinositol 4,5-bisphosphate (PIP_2) and blocks recruitment of AKT kinases to the plasma membrane[28–31]. Mutations in components of this pathway lead to changes in lifespan, development, metabolism and stress responses in *C. elegans*[32,33]. In addition, loss-of-function (*lf*) mutations in the *akt-1* and *akt-2* genes cause hypersensitivity to ionizing radiation–induced germ-cell apoptosis[34], thus suggesting that AKT kinases also have a prosurvival role in *C. elegans*.

In this study, we set out to understand how caspases inactivate cell-survival factors to promote apoptosis, and we demonstrate a new mechanism that inactivates AKT kinases. CNT-1, upon cleavage by CED-3, generates tCNT-1, which in turn acquires a potent phosphoinositide (PI)-binding activity and translocates from the cytoplasm to the plasma membrane, where it outcompetes AKT kinases for binding to PIP_3, suppresses the PI3K-AKT cell-survival pathway and promotes apoptosis.

Department of Molecular, Cellular and Developmental Biology, University of Colorado, Boulder, Boulder, Colorado, USA. Correspondence should be addressed to D.X. (ding.xue@colorado.edu).

Received 2 May; accepted 14 October; published online 10 November 2014; doi:10.1038/nsmb.2915

RESULTS

CNT-1 promotes apoptosis downstream of CED-3

To identify genes encoding proteins acting downstream of CED-3 to kill cells, we performed a genetic screen to isolate suppressors of ectopic neuronal death induced by activated CED-3 (acCED-3)[35] and isolated a recessive mutation, *sm8*, which defines a new gene *cps-2* (CED-3 protease suppressor) on linkage group (LG) II (Online Methods).

We investigated whether *cps-2* affects apoptosis by examining embryonic cell death in *cps-2*(*sm8*) animals. Compared with wild type N2 embryos, *cps-2*(*sm8*) embryos had fewer apoptotic cell corpses in the early stages of embryogenesis (comma and 1.5-fold stages) and more cell corpses in later stages (**Fig. 1a**), displaying a characteristic delay-of-cell-death phenotype observed in mutants defective in genes encoding proteins acting downstream of CED-3 (refs. 7,35–37). Three-point mapping and single-nucleotide polymorphism (SNP) mapping placed *cps-2*(*sm8*) at a position of 12103628 bp on LGII (**Fig. 1b**). Because there are no available fosmid or cosmid clones in this region for transformation rescue experiments, we performed an RNA interference (RNAi) screen on nine candidate genes in this region and found that RNAi knockdown of *cnt-1* caused a similar delay-of-cell-death defect (**Supplementary Table 1**). We then introduced into *cps-2*(*sm8*) animals a *cnt-1* minigene containing a full-length *cnt-1* cDNA fused to 1,944 bp of the *cnt-1* promoter and found that it rescued the *cps-2*(*sm8*) defect (**Fig. 1b** and **Supplementary Fig. 1a**). Moreover, an existing *cnt-1*–deletion mutation (*tm2313*) caused a similar delay-of-cell-death defect and failed to complement *cps-2*(*sm8*) (**Fig. 1a**), thus indicating that *tm2313* and *sm8* are allelic. Sequencing analysis of *cps-2*(*sm8*) animals revealed a nucleotide deletion at 927 bp upstream from the *cnt-1* translational start but no mutation in the coding region of *cnt-1* and the 1,031-bp 3′ untranslated region. Because a *cnt-1* minigene carrying this nucleotide deletion failed to rescue the cell-death defect in *cps-2*(*sm8*) animals (**Fig. 1b** and **Supplementary Fig. 1a**) and because neither *cnt-1* mRNA nor CNT-1 protein was detectable in *cps-2*(*sm8*) animals (**Supplementary Fig. 1b**,**c**), *sm8* probably disrupts a *cis* element important for *cnt-1* expression. These results indicate that *cps-2* is *cnt-1*. *cnt-1(tm2313)* was thus used in all subsequent experiments.

We examined whether delay of cell death caused by *cnt-1(tm2313)* results in survival of cells that normally die, yielding extra 'undead' cells in the anterior pharynxes of mutant animals[35]. Like wild-type animals, *cnt-1(tm2313)* animals had few extra undead cells (**Supplementary Table 2**). However, in sensitized backgrounds such as in animals weakly defective in *ced-3* and *ced-4*, *cnt-1(tm2313)* significantly increased the numbers of extra cells observed in these weak-cell-death mutants, thus indicating that *cnt-1* promotes apoptosis.

Because *sm8* inhibits acCED-3–induced neuronal death, we examined whether CNT-1 functions downstream of CED-3, using an integrated transgene (*smIs111*) expressing acCED-3 from the *egl-1* promoter[38]. The cell death–initiating EGL-1 functions upstream of CED-3 to induce apoptosis and is mainly expressed in dying cells[39]. When we placed *smIs111* in the *ced-4(n1162)* mutant, in which almost all physiological cell death is blocked, acCED-3 still induced ectopic cell death (**Fig. 1c**). *cnt-1(tm2313)* significantly reduced the number of ectopic deaths in *smIs111; ced-4(n1162)* embryos, thus indicating that CNT-1 is likely to act downstream of CED-3 to promote apoptosis.

CNT-1 is cleaved sequentially at two sites by CED-3

Given that CNT-1 acts downstream of CED-3, we tested whether CNT-1 is a substrate of CED-3 protease. We incubated an ^{35}S-methionine–labeled glutathione S-transferase (GST) fusion of the longer CNT-1 isoform, GST–CNT-1a, with CED-3 and found that it was cleaved by CED-3 to yield two species of approximately 68 and 24 kDa (**Fig. 2a**). Because GST–CNT-1a is 116 kDa, this cleavage pattern suggests that the 24-kDa species might contain two cleavage products of similar sizes and that CNT-1a is cleaved at two different sites. From the consensus CED-3–cleavage sites (DXXD, with X representing any amino acid)[40], we identified three potential CED-3–cleavage sites: Asp382 (DSVD), Asp508 (DSID) and Asp609 (DVQD). We then generated aspartate-to-glutamate substitutions in each potential cleavage site (D1, D2 and D3) and tested CED-3 cleavage of the mutant proteins. The D1E mutation completely abolished cleavage of CNT-1a by CED-3 (**Fig. 2a**), thus suggesting that D1 is required for CED-3 cleavage. The D2E mutation did not alter the cleavage pattern (**Fig. 2a**), a result indicating that D2 is not a CED-3–cleavage site *in vitro*. The D3E mutation abolished the 24-kDa species and instead produced a new 47-kDa band along with the 68-kDa band (**Fig. 2a**), thus confirming that CED-3 cleavage at D3 generates two cleavage products of similar sizes (23 and 24 kDa). Because D1E also blocked cleavage at the D3 site, CED-3 cleavage at the D1 site is required for cleavage at the D3 site. In CNT-1b—a shorter isoform of CNT-1 that

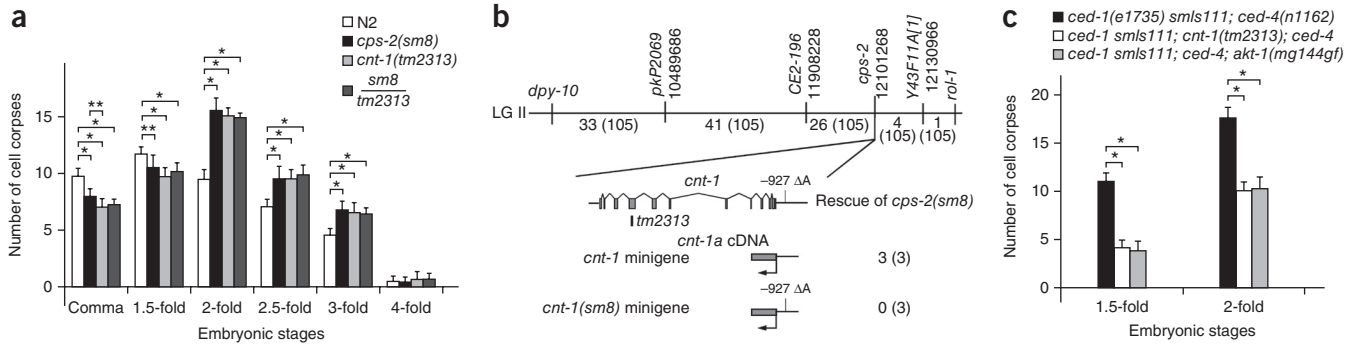

Figure 1 Cloning and characterization of *cps-2*. (**a**) Embryonic cell corpses counted in animals with the indicated genotypes. (**b**) Mapping and cloning of *cps-2*. Top, genetic map with two genetic markers (*dpy-10* and *rol-1*) and three SNPs (*pkP2069*, *CE2-196* and *Y43F11A[1]*) used for mapping *cps-2(sm8)*. Numbers below are the numbers of recombination events (out of 105 total) that occurred between two genetic markers and three SNPs. Bottom, the *cnt-1* coding region, the *sm8* mutation, the *tm2313* deletion and the results of rescue of the *cps-2(sm8)* mutant by the $P_{cnt\text{-}1}$CNT-1a::3×Flag and $P_{cnt\text{-}1(sm8)}$CNT-1a::3×Flag constructs. Three independent transgenic arrays (numbers inside parentheses) were examined for each rescue experiment, and the number of arrays that rescued the cell-death defect of *cps-2(sm8)* is indicated. ΔA indicates the A nucleotide deleted in *cps-2(sm8)*. (**c**) Embryonic cell corpses counted in animals with the indicated genotypes. In **a** and **c**, average number of cell corpses ±s.d. (n = 15 embryos at each stage) are shown. $^*P < 0.001$; $^{**}P < 0.05$ by two-way ANOVA followed by Bonferroni comparison.

© 2014 Nature America, Inc. All rights reserved.

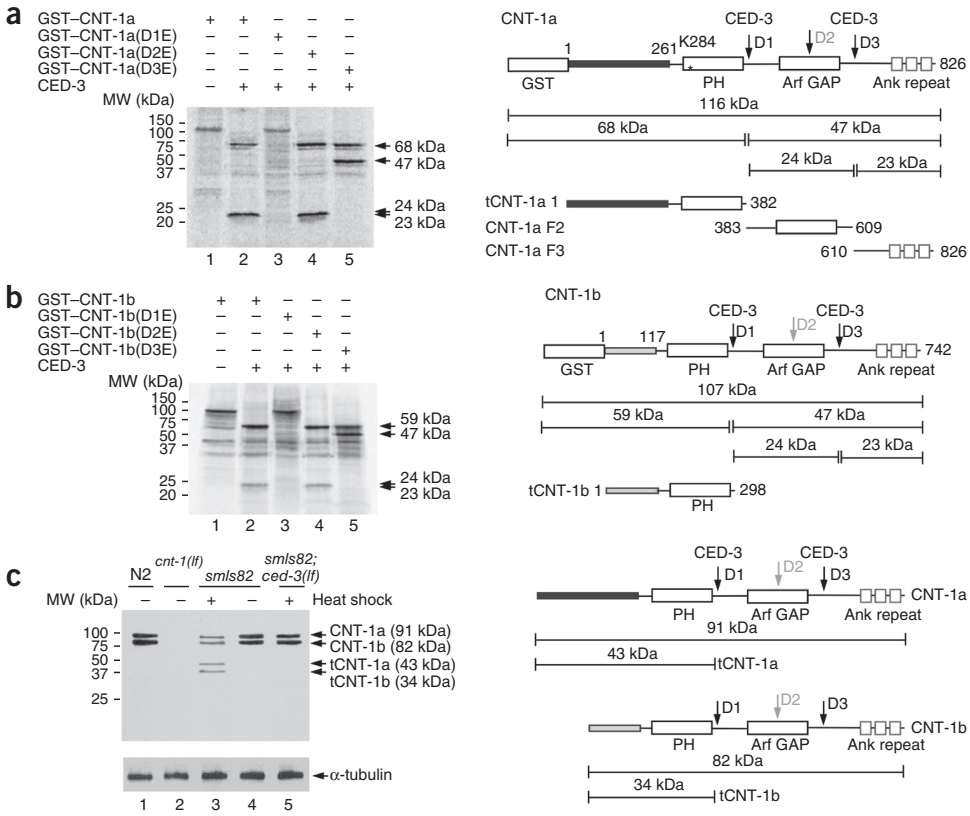

Figure 2 Cleavage of CNT-1 by CED-3 *in vitro* and *in vivo*. (**a**) CED-3–cleavage assay of GST–CNT-1a. ^{35}S-methionine–labeled GST–CNT-1a and its mutant derivatives incubated with or without CED-3, resolved by 15% SDS-PAGE gel. CED-3–cleavage products are indicated by arrows. Right, schematic diagram of GST–CNT-1a and sizes of the CED-3–cleavage products (tCNT-1a, CNT-1a F2 and CNT-1a F3). Three predicted CED-3–cleavage sites are indicated with arrows. The black box at the N terminus represents the region that is different from CNT-1b. The lysine residue in the PH domain (K284) critical for lipid binding is indicated with an asterisk. (**b**) CNT-1b cleavage by CED-3. Left, GST–CNT-1b and its mutant derivatives synthesized, labeled, digested with CED-3 and resolved on SDS-PAGE as in **a**. Right, schematic diagram of GST–CNT-1b with the sizes of the CED-3–cleavage products indicated. The gray box at the N terminus represents the region that is different from CNT-1a. (**c**) Left, immunoblotting analysis of *C. elegans* embryos, showing CED-3–mediated cleavage of CNT-1 *in vivo*. Samples are from embryos with the indicated genotypes, treated with or without heat shock, lysed and resolved on SDS-PAGE (Online Methods). Antibodies used are anti–CNT-1 antibody (top) or an anti–α-tubulin antibody (loading control; bottom). (Uncropped image is in **Supplementary Fig. 1e**.) Right, schematic diagram of CNT-1a, tCNT-1a, CNT-1b and tCNT-1b and their sizes. Ank, ankyrin; GAP, GTPase-activating protein; MW, molecular weight.

has the same 564–amino acid C terminus, including a PH domain, but a different 177-residue N-terminal sequence (**Fig. 2b**)—we found three identical CED-3–cleavage sites (Asp298, Asp424 and Asp525). We observed similar CED-3–cleavage patterns with GST–CNT-1b and GST–CNT-1b mutants carrying D1E, D2E or D3E (**Fig. 2b**). These data indicate that D1 is the primary CED-3–cleavage site in CNT-1 and is required for subsequent CED-3 cleavage at D3.

To examine whether CNT-1 is a CED-3 substrate *in vivo*, we probed for CNT-1–cleavage products in worm lysates by using an antibody raised against the N-terminal cleavage product of CNT-1b (tCNT-1b), which recognizes recombinant tCNT-1b and tCNT-1a (**Supplementary Fig. 1d**). In wild-type animals, we detected two bands consistent with the sizes of full-length CNT-1a and CNT-1b, which were absent in the *cnt-1(tm2313)* mutant (**Fig. 2c**). The observed absence of cleaved CNT-1 products is because little apoptosis occurs in wild-type embryos. In animals carrying an integrated transgene (*smIs82*) that induces global expression of death initiator EGL-1 and widespread apoptosis under the control of heat-shock promoters (P_{hsp}EGL-1)[6], the same two bands were present before heat-shock treatment (**Fig. 2c**). After heat-shock treatment, the intensity of these two bands was reduced, and two smaller bands consistent with the sizes of tCNT-1a and tCNT-1b appeared. The appearance of the tCNT-1a and tCNT-1b bands was CED-3 dependent, because a *ced-3(n717) lf* mutation abolished these two bands in *smIs82* animals. Therefore, CNT-1 is cleaved by CED-3 in *C. elegans*.

Cleavage of CNT-1 activates tCNT-1 proapoptotic activity

We determined whether CNT-1 cleavage by CED-3 is important for apoptosis (**Fig. 3**). Expression of CNT-1a or CNT-1b from a globally active *dpy-30* promoter ($P_{dpy\text{-}30}$) fully rescued the delay-of-cell-death defect in *cnt-1(tm2313)* animals (**Fig. 3a** and **Supplementary Fig. 2a**). However, $P_{dpy\text{-}30}$CNT-1a(D1E) and $P_{dpy\text{-}30}$CNT-1b(D1E), expressing CNT-1 mutants resistant to CED-3 cleavage, did not rescue the *cnt-1(tm2313)* mutant (**Fig. 3b** and **Supplementary Fig. 2b**), thus indicating that cleavage of CNT-1 by CED-3 is critical for its proapoptotic function. Expression of tCNT-1a or tCNT-1b at 20% of the endogenous CNT-1 level (**Supplementary Fig. 2c,d**) led to increased cell death in most embryonic stages compared to that in wild type and *cnt-1(tm2313)* embryos (**Fig. 3c** and **Supplementary Fig. 2e**). The increased numbers of cell corpses observed in animals carrying $P_{dpy\text{-}30}$tCNT-1a or $P_{dpy\text{-}30}$tCNT-1b were due to ectopic cell death, because some pharyngeal cells that normally live were randomly lost in transgenic larvae (**Supplementary Table 3**). In comparison, coexpression of the other two CNT-1a CED-3–cleavage fragments, CNT-1a F2 and CNT-1a F3 (**Fig. 2a**), did not induce ectopic cell death or rescue the *cnt-1(tm2313)* mutant (**Fig. 3d**), whereas coexpression of all three CED-3–cleavage products did (**Supplementary Fig. 2f**). These results indicate that tCNT-1, activated by CED-3 cleavage, is responsible for CNT-1's proapoptotic activity.

CNT-1 promotes cell death by inhibiting the AKT pathway

Because the only recognizable motif in tCNT-1 is the PH domain (**Fig. 2**), a potential PI-binding domain[41], and because one of the PI species, PIP_3, activates AKT kinases (also containing a PH domain) to promote cell survival[8,9], we asked whether *C. elegans* AKT kinases participate in regulating apoptosis and genetically interact with *cnt-1*. An activating mutation in *akt-1*, *akt-1(mg144gf)*[22], caused a delay-of-cell-death defect similar to that of the *cnt-1(tm2313)* mutant

© 2014 Nature America, Inc. All rights reserved.

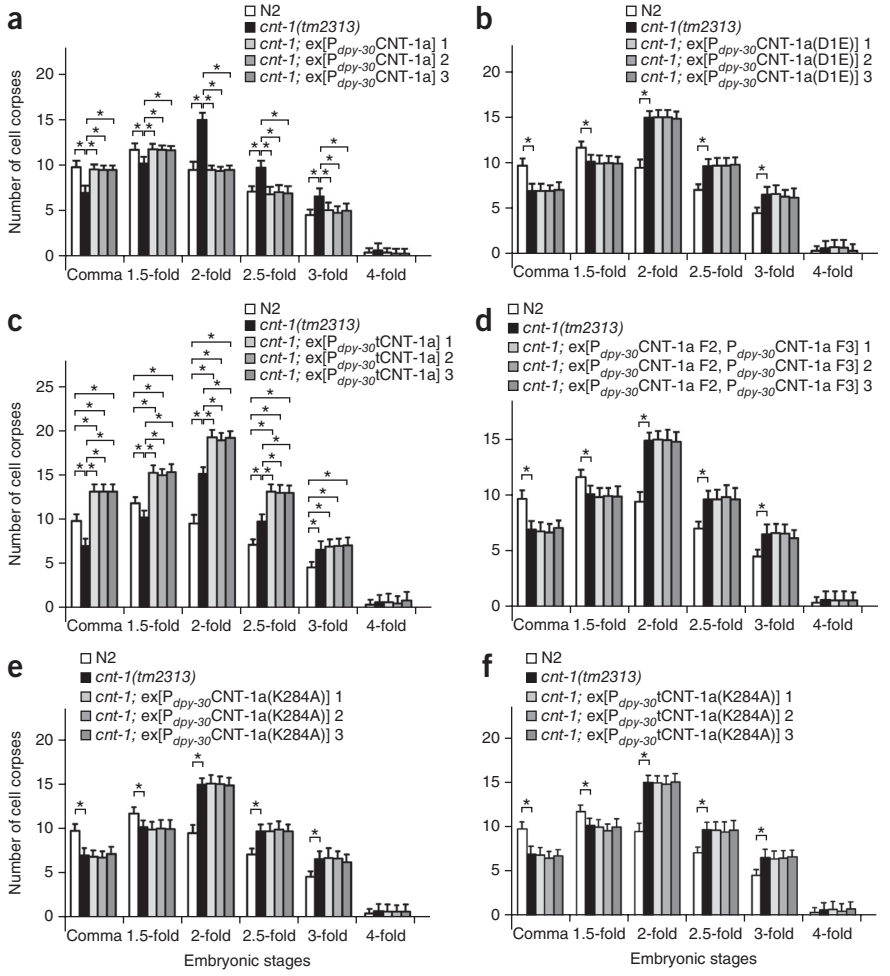

Figure 3 Cleavage of CNT-1 by CED-3 activates its proapoptotic activity. Cell corpses scored in embryos with the indicated genotypes, at the indicated embryonic stages. Embryos carrying three independent extrachromosomal arrays (ex) were scored. The average number of cell corpses ±s.d. ($n = 15$ embryos at each stage) are shown. $^*P < 0.001$ by two-way ANOVA followed by Bonferroni comparison.

(**Fig. 4a**). Combination of *cnt-1(tm2313)* and *akt-1(mg144gf)* did not enhance this phenotype, thus suggesting that AKT-1 and CNT-1 function in the same pathway. Because the *ced-3(n2438); akt-1(mg144gf)* double mutant had more extra undead cells than *ced-3(n2438)* or *akt-1(mg144gf)* single mutants (**Supplementary Table 4**), this suggests that AKT-1 inhibits cell death. Epistasis analysis with animals carrying a $P_{dpy\text{-}30}$tCNT-1a transgene showed that *akt-1(mg144gf)* completely blocked ectopic cell death induced by $P_{dpy\text{-}30}$tCNT-1a (**Fig. 4b**), a result indicating that AKT-1 probably acts downstream of CNT-1 to inhibit cell death. In agreement with this result, *akt-1(mg144gf)* suppressed ectopic cell death induced by *smIs111*, a transgene expressing acCED-3, to the same extent as *cnt-1(tm2313)* (**Fig. 1c**), thus indicating that AKT-1 can act downstream of CED-3 to promote cell survival.

We also examined animals carrying a *lf* mutation in *akt-1*, *akt-2* or *sgk-1*, encoding three AKT kinases acting in parallel in the IIS pathway[22,23]. *akt-1(tm399)*, *akt-2(tm1075)* and *sgk-1(ok538)* each did not cause a detectable cell death defect, whereas all three combinations of double mutations and the triple mutation combination caused increased cell death throughout embryogenesis (**Supplementary Fig. 3a**), thus indicating that the presence of at least two AKT and SGK kinases is important for cell survival. Because *cnt-1(tm2313)* failed to suppress ectopic cell death in the triple mutant (**Fig. 4c** and **Supplementary Table 5**), these results suggest that CNT-1 functions upstream of AKT-1, AKT-2 and SGK-1 to promote cell death.

AKT kinases phosphorylate proteins to transduce signals in various pathways[22,42,43]. To examine whether the kinase activity of AKT is important for its antiapoptotic activity, we expressed kinase-defective mutants of AKT-1 and AKT-2, AKT-1(K222M) and AKT-2(K209M), in the *akt-1(tm399); akt-2(tm1075)* mutant[22]. Expression of wild-type AKT-1 or AKT-2 rescued the increased-cell-death phenotype of the *akt-1(tm399); akt-2(tm1075)* mutant, whereas expression of AKT-1 (K222M) or AKT-2(K209M) did not (**Supplementary Fig. 4a**,**b**), thus indicating that the kinase activity of AKT is required for its prosurvival function.

A key substrate of AKT kinases in the IIS pathway is DAF-16, a homolog of the FOXO transcriptional factor[24,25,42]. A *daf-16 lf* mutation, *mu86*, caused a delay-of-cell-death defect similar to that of *cnt-1(tm2313)* or *akt-1(mg144gf)* animals but did not enhance their cell-death defects (**Supplementary Fig. 3b**,**c**), thus indicating that DAF-16, AKT-1 and CNT-1 function in the same pathway to affect apoptosis. Moreover, *daf-16(mu86)* fully suppressed ectopic cell death induced by tCNT-1a (**Supplementary Fig. 3d**) and increased the number of extra undead cells in *ced-3(n2438)* animals (**Supplementary Table 4**), suggesting that DAF-16 acts downstream of CNT-1 to promote cell death.

CNT-1 acts downstream of PI3K to promote cell death

C. elegans AKT kinases are activated by PIP_3 and therefore are regulated by AGE-1, a PI3K that phosphorylates PIP_2 to generate PIP_3 (refs. 19,20). An *age-1(mg44) lf* mutation caused an increased-cell-death phenotype similar to that of *akt-1(tm399); akt-2(tm1075) sgk-1(ok538)* animals (**Fig. 4c**,**d**) but did not enhance the increased-cell-death phenotype caused by $P_{dpy\text{-}30}$tCNT-1a (**Supplementary Fig. 3e**), thus suggesting that AGE-1 inhibits and tCNT-1 promotes apoptosis in the same pathway. Conversely from what we observed with the *akt-1(lf); akt-2(lf) sgk-1(lf)* triple mutant (**Fig. 4c**), *cnt-1(tm2313)* blocked both the increased cell death and the missing-cell phenotypes caused by *age-1(mg44)* (**Fig. 4d** and **Supplementary Table 5**), thus indicating that CNT-1 probably acts downstream of AGE-1 to promote apoptosis.

PIP_3 is dephosphorylated and converted to PIP_2 by the PTEN phosphatase[8,9], which is encoded by *daf-18* in *C. elegans*[28–31]. The *daf-18(e1375) lf* mutation caused a delay-of-cell-death phenotype similar to that of *cnt-1(tm2313)* animals (**Fig. 4e**) and did not exacerbate the *cnt-1(tm2313)* cell-death defect, thus suggesting that DAF-18 and CNT-1 act in the same pathway. *daf-18(e1375)* also increased the number of extra cells in *ced-3(n2438)* animals (**Supplementary Table 4**). *daf-18(e1375)*, however, did not block ectopic cell death induced by tCNT-1a (**Fig. 4f**), a result indicating that DAF-18 acts upstream of, or in parallel to, CNT-1 to promote cell

© 2014 Nature America, Inc. All rights reserved.

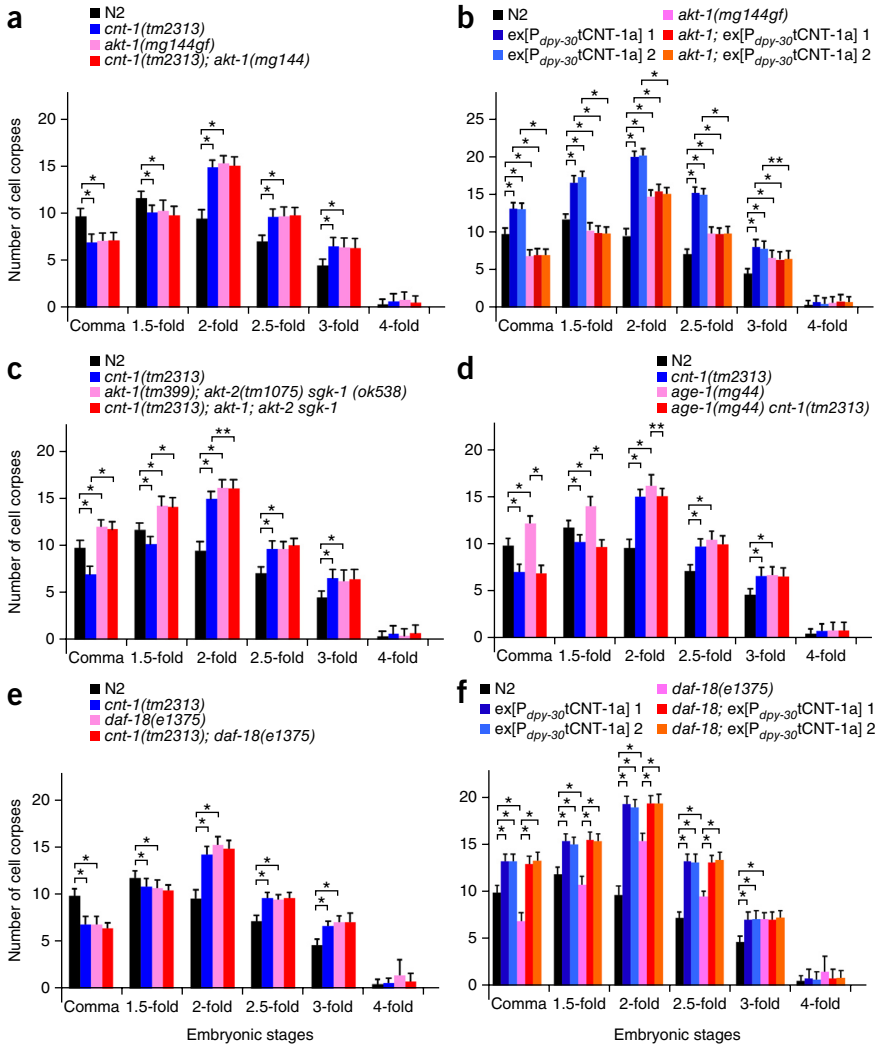

Figure 4 CNT-1 acts downstream of AGE-1 but upstream of AKT-1, AKT-2 and SGK-1 to promote apoptosis. Cell corpses scored in the indicated strains as in **Figure 3**. Embryos carrying two independent extrachromosomal arrays were scored (**b**,**f**). Average number of cell corpses ±s.d. (n = 15 embryos at each stage) are shown. $^{*}P < 0.001$; $^{**}P < 0.05$ by two-way ANOVA followed by Bonferroni comparison.

death, possibly at the level of PIP_3 regulation. When taken together, our results suggest that CNT-1 and DAF-18 act in the same pathway to promote cell death and that CNT-1 operates downstream of AGE-1 and upstream of AKT-1, AKT-2, SGK-1 and DAF-16.

Cleavage of CNT-1 activates its PI binding

Given that AGE-1 activates AKT kinases through PIP_3, and DAF-18 inactivates this pathway through dephosphorylation of PIP_3, we hypothesized that tCNT-1, with a PH domain, promotes cell death by interfering with the binding of PIP_3 by AKT kinases. We examined whether tCNT-1 binds PIP_3 by using an *in vitro* lipid binding assay. ^{35}S-methionine–labeled GST–CNT-1a on its own did not bind any lipid but showed strong binding to PIP, PIP_2 and PIP_3 and weak binding to phosphatidic acid and cardiolipin after pretreatment with CED-3 (**Fig. 5a**). GST–tCNT-1a displayed an identical lipid binding pattern to that of CED-3–treated GST–CNT-1a (**Fig. 5a**), and so did GST–CNT-1b pretreated with CED-3 and GST–tCNT-1b (**Fig. 5a**). When we altered one of the highly conserved PI-binding lysine residues in the PH domain of CNT-1a (K284A)[44], neither CNT-1a(K284A) pretreated with CED-3 nor tCNT-1a(K284A) showed any lipid binding activity (**Fig. 5a**). Moreover, expression of CNT-1a(K284A) or tCNT-1a(K284A) in *cnt-1(tm2313)* animals did not rescue the cell-death defect or cause ectopic cell death (**Fig. 3e**,**f**). Because the K284A mutation did not alter the expression levels of CNT-1a proteins *in vitro* or *in vivo* (**Supplementary Fig. 5**), these results indicate that the PH domain is required for tCNT-1 to acquire PI binding after CED-3 cleavage and to promote apoptosis.

tCNT-1 blocks PIP_3 binding by AKT and SGK kinases

We tested whether tCNT-1 interferes with binding of AKT and SGK kinases to PIP_3 (refs. 21–23). ^{35}S-methionine–labeled AKT-1 alone bound strongly to PIP_3 and weakly to cardiolipin, and this binding was not affected by addition of unlabeled GST–CNT-1a or GST–CNT-1b (**Fig. 5b**). Addition of GST–CNT-1a or GST–CNT-1b pretreated with CED-3 completely blocked PIP_3 binding by AKT-1 (**Fig. 5b**), whereas incubation of AKT-1 with CED-3 did not alter AKT-1 lipid binding (**Fig. 5b**). Likewise, both AKT-2 and SGK-1 bound strongly to PIP_3, and this binding was blocked by GST–CNT-1a pretreated with CED-3 (**Fig. 5c**). To probe how tCNT-1 inhibits PIP_3 binding by AKT-1, we compared their PIP_3 binding affinity. We first determined the concentrations of ^{35}S-methionine–labeled GST–tCNT-1a and AKT-1 synthesized in rabbit reticulocyte lysate (RRL) by comparing them with known concentrations of recombinant GST–tCNT-1a and AKT-1 proteins, which were purified from bacteria and showed no lipid binding activity (**Fig. 6a**). Labeled GST–tCNT-1a and hexahistidine (His_6)-tagged AKT-1 displayed comparable radioactive-signal intensity at the same concentrations (**Fig. 6b**). GST–tCNT-1a displayed strong PIP_3 binding at 0.04 nM, weak binding at 0.004 nM and no binding at 0.0004 nM (**Fig. 6c**). By contrast, AKT-1 showed strong PIP_3 binding at 4 nM, weak binding at 0.4 nM and no binding at 0.04 nM (**Fig. 6c**), results indicating that tCNT-1a binds PIP_3 with an affinity two orders of magnitude higher than that of AKT-1. Because the expression level of CNT-1 in *C. elegans* is approximately 70% higher than that of AKT-1 (**Supplementary Fig. 6**), the combination of higher CNT-1 concentrations and much higher binding affinity to PIP3 than those of AKT-1 allows tCNT-1 to block PIP_3 binding by AKT kinases and thus block their activation.

tCNT-1 translocates to the plasma membrane upon CED-3 cleavage

Several proteins containing the PH domain translocate from the cytosol to the plasma membrane via a PIP_3-mediated mechanism[45–47]. We analyzed the subcellular localization of CNT-1 by using an antibody raised against tCNT-1b (**Supplementary Fig. 1d**). CNT-1 localized in the cytoplasm of all cells in wild-type embryos (**Fig. 7a**) but was not detectable in *cnt-1(tm2313)* embryos (**Fig. 7b**), thus demonstrating the specificity of the antibody. In *smIs82* (P_{hsp}EGL-1)

© 2014 Nature America, Inc. All rights reserved.

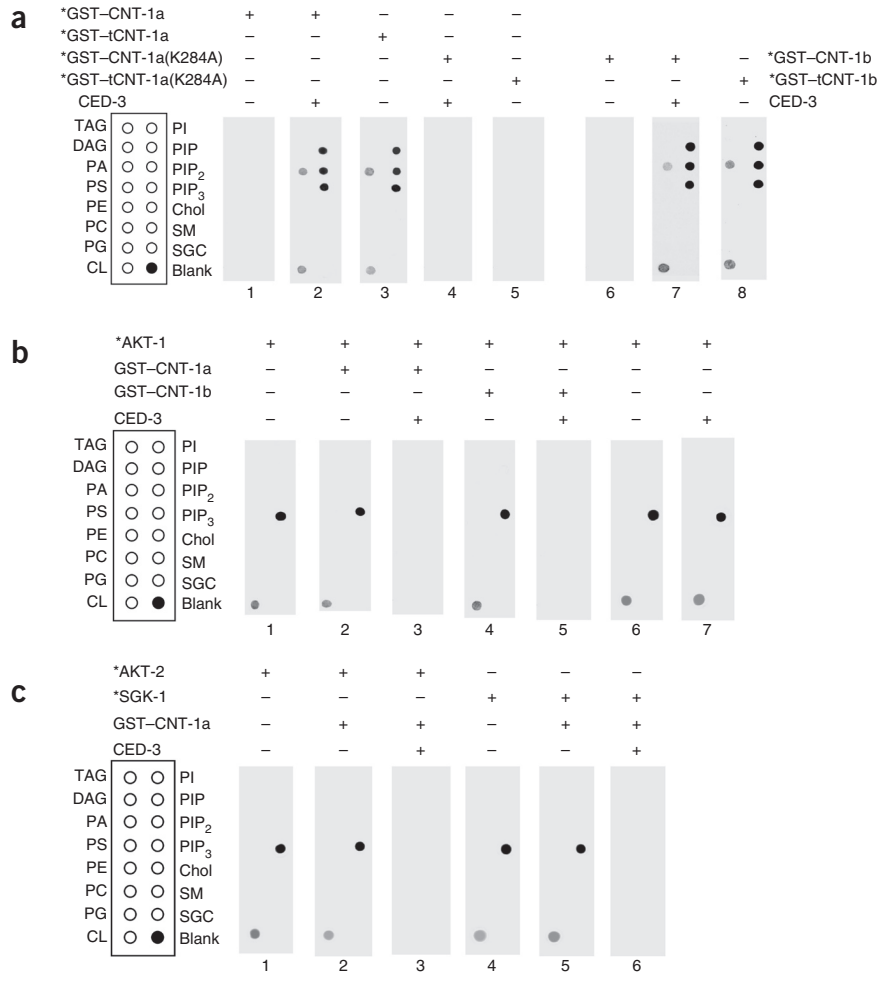

Figure 5 CED-3–activated PI binding of CNT-1 blocks PIP_3 binding by AKT and SGK kinases. (**a**) Lipid binding assays of CNT-1 in the presence of CED-3. The indicated proteins labeled with ^{35}S-methionine (*) were first incubated with or without CED-3 and then added to the membrane strips shown (Online Methods). (**b**) AKT-1 lipid binding assay in the presence of CNT-1 and CED-3. Unlabeled GST–CNT-1a and GST–CNT-1b were incubated with CED-3 and then added with radiolabeled AKT-1(*) to the membrane strips (Online Methods). (**c**) AKT-2 and SGK-1 lipid binding assay in the presence of CNT-1 and CED-3. Radiolabeled (*) AKT-2 and SGK-1 were incubated with membrane strips as described in **b**. In all panels, lipids spotted on the strips are TAG, triacylglycerol; DAG, diacylglycerol; PA, phosphatidic acid; PS, phosphatidylserine; PE, phosphatidylethanolamine; PC, phosphatidylcholine; PG, phosphatidylglycerol; CL, cardiolipin; PI, phosphatidylinositol; PIP, phosphatidylinositol (4)-phosphate; PIP_2, phosphatidylinositol (4,5)-bisphosphate; PIP_3, phosphatidylinositol (3,4,5)-trisphosphate; chol, cholesterol; SM, sphingomyelin; SGC, 3-sulfogalactosylceramide.

embryos in which we induced global apoptosis and widespread CED-3 activation through heat-shock treatment, we observed CNT-1 staining on the plasma membranes of all cells in addition to staining in the cytoplasm (**Fig. 7d** and **Supplementary Fig. 7c**,**d**), results indicating that a portion of CNT-1 translocated from the cytosol to the plasma membrane upon apoptosis activation. By contrast, in *smIs82* embryos without heat-shock treatment or in *smIs82; ced-3(n717)* embryos with heat-shock treatment, CNT-1 remained in the cytoplasm (**Fig. 7c**,**e** and **Supplementary Fig. 7a**,**b**,**e**,**f**), thus indicating that CNT-1 translocation from the cytosol to the plasma membrane is dependent on apoptosis and CED-3. In *cnt-1(tm2313); smIs82* embryos expressing CNT-1a(D1E), the CED-3–uncleavable form of CNT-1a, CNT-1a(D1E) did not translocate to the plasma membrane after heat-shock treatment (**Supplementary Fig. 7g–i**). In contrast, in *cnt-1(tm2313); smIs82* embryos expressing CNT-1a, we observed CNT-1a on plasma membranes after heat-shock treatment (**Supplementary Fig. 7j–l**). These results confirm that CED-3 cleavage is required for CNT-1 translocation to the plasma membrane during apoptosis. Consistently with this, loss of *cnt-1* partially suppressed and e xpression of tCNT-1a enhanced ectopic cell death induced by *smIs82* (**Supplementary Note** and **Supplementary Fig. 4c**,**d**), thus providing further support to the finding that cleavage of CNT-1 and activation of tCNT-1 is an important downstream event of CED-3 activation and apoptosis.

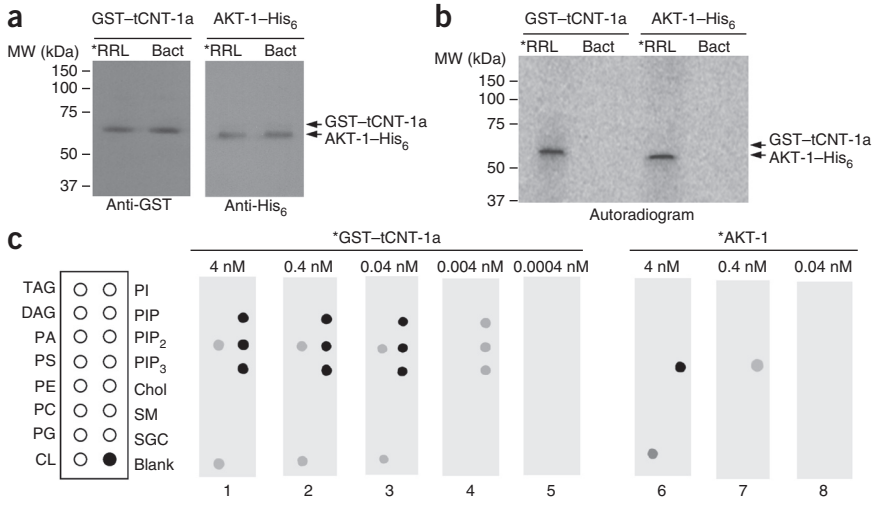

Figure 6 PIP_3 binding activity of tCNT-1a is two orders of magnitude greater than that of AKT-1. (**a**) Immunoblotting of 5.1 µl of GST–tCNT-1a and 2.9 µl of AKT-1–His_6 proteins synthesized and radiolabeled in rabbit reticulocyte lysate (*RRL) and 1 pmol of GST–tCNT-1a or AKT-1–His_6 proteins purified from bacteria (Bact) with anti-GST or anti-His_6 antibodies (Online Methods). (**b**) Autoradiogram of 1 pmol of ^{35}S-methionine–labeled GST–tCNT-1a and AKT-1–His_6 proteins made in RRL, showing comparable radioactive-signal intensity. (**c**) Lipid binding assays of GST–tCNT-1a or AKT-1–His_6. Radiolabeled (*) GST–tCNT-1a or AKT-1–His_6 at the indicated concentrations were incubated with lipid membrane strips as described in **Figure 5**.

© 2014 Nature America, Inc. All rights reserved.

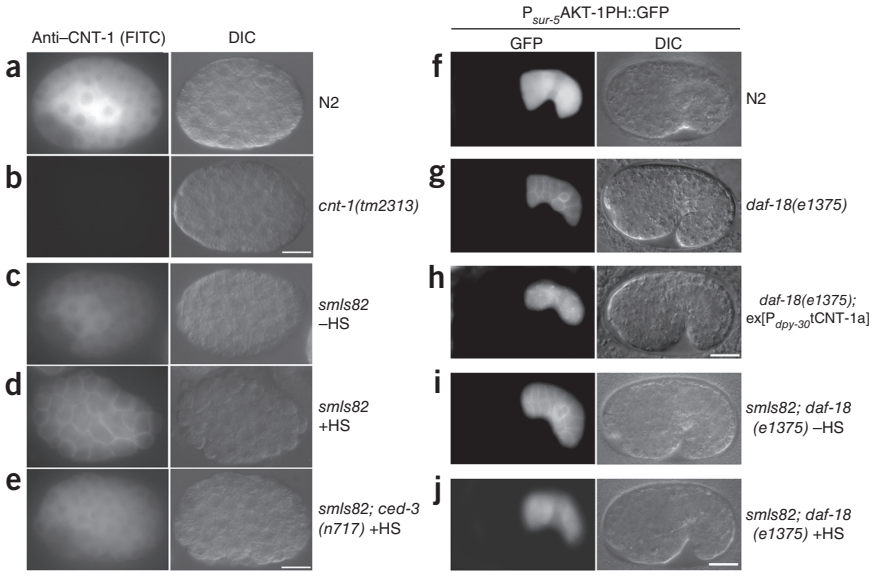

Figure 7 CED-3–dependent translocation of CNT-1 to the plasma membrane blocks AKT-1 membrane recruitment. (**a**–**e**) Immunostaining of CNT-1 in *C. elegans* embryos with the indicated genotypes, with or without heat-shock treatment as indicated. Fluorescein isothiocyanate (FITC, left) and differential interference contrast (DIC, right) images of the stained embryos are shown. –HS, no heat-shock treatment; +HS, with heat-shock treatment. (**f**–**j**) Microscopy analysis of AKT-1-PH::GFP localization in *C. elegans* embryos with the indicated genotypes, with or without heat-shock treatment. All strains contained the same ex[$P_{sur\text{-}5}$AKT-1-PH::GFP] transgenic array. GFP (left) and DIC (right) images of transgenic embryos are shown. Scale bars, 10 μm.

tCNT-1 inhibits association of AKT-1 with the plasma membrane

AKT-1 also contains a PH domain, and its human homolog translocates to the plasma membrane through binding to PIP_3 (ref. 48). Given the limited amount of PIP_3 on the plasma membrane, the higher concentration of CNT-1 than AKT-1 *in vivo* and the much-stronger PIP_3 binding affinity of tCNT-1 than AKT-1, we examined whether tCNT-1 blocks AKT-1 translocation to the plasma membrane. We fused the first 180 residues of AKT-1, including its PH domain (residues 15–118), to GFP and expressed it from the *sur-5* gene promoter ($P_{sur\text{-}5}$AKT-1-PH::GFP). In wild-type embryos carrying $P_{sur\text{-}5}$AKT-1-PH::GFP, GFP was diffuse within the cells (**Fig. 7f**). When we crossed this transgene into *daf-18(e1375)* animals, which are deficient in converting PIP_3 to PIP_2 and thus have elevated levels of PIP_3 in the plasma membrane, we saw bright GFP signals on the plasma membrane, thus suggesting that AKT-1-PH::GFP translocated to the plasma membrane through binding to PIP_3 (**Fig. 7g**). Expression of tCNT-1a abolished AKT-1-PH::GFP localization to the plasma membrane in *daf-18(e1375)* embryos (**Fig. 7h**), thus indicating that tCNT-1 inhibited association of AKT-1 with the plasma membrane. Similarly, in *smIs82; daf-18(e1375)* animals carrying $P_{sur\text{-}5}$AKT-1-PH::GFP, some AKT-1-PH::GFP localized to the plasma membrane in the absence of heat-shock treatment (**Fig. 7i**). After heat-shock treatment, AKT-1-PH::GFP disappeared from the plasma membrane (**Fig. 7j**), a result indicating that endogenous tCNT-1 induced by *smIs82* is sufficient to block AKT-1 association with the plasma membrane and thus block AKT-1 activation and function.

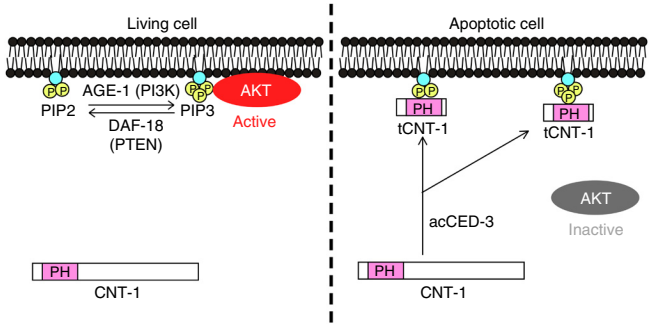

Figure 8 A model of CED-3–activated suppression of AKT signaling by CNT-1 in *C. elegans*. In nonapoptotic cells, some AKT kinases are recruited to the plasma membrane and are activated by PIP_3 to transduce the survival signal. In apoptotic cells, CNT-1 is cleaved by activated CED-3 to generate potent PI-binding tCNT-1, which translocates to the plasma membrane from the cytoplasm. tCNT-1 outcompetes AKT kinases for binding to PIP_3 and thus displaces and inactivates AKT kinases to lead to loss of the survival signal and apoptosis.

DISCUSSION

The physiological relevance of caspase substrates is an under-studied area that limits the understanding of apoptosis. We have identified multiple components acting downstream of CED-3 to promote apoptosis, using a sensitized CED-3 protease suppressor (*cps*) screen[35]. The cell-death defects of each *cps* mutant are mild or undetectable because multiple pathways downstream of CED-3 act in parallel to kill the cell[5–7,35]. In this study, we characterized one of the *cps* genes, *cps-2 (cnt-1)*, whose inactivation delays cell death and suppresses apoptosis in sensitized genetic backgrounds. Importantly, CNT-1 is a substrate of CED-3 both *in vitro* and *in vivo*. A mutation blocking CNT-1 cleavage by CED-3 abolishes its proapoptotic activity, whereas tCNT-1 alone is sufficient to induce apoptosis. These results establish that CNT-1 is an *in vivo* CED-3 target.

Despite containing a PH domain, a potential PI-binding motif, CNT-1 does not bind any phospholipids *in vitro* or associate with the plasma membrane *in vivo*. Upon activation by CED-3 cleavage during apoptosis, tCNT-1 acquires strong binding to PIs and translocates to the plasma membrane, where it outcompetes AKT kinases for PIP_3 binding to block recruitment and activation of AKT kinases at the plasma membrane, thereby inactivating the AKT survival pathway to accelerate cell killing (**Fig. 8**). Therefore, CED-3 activates a downstream death-execution event by cleaving CNT-1, which then inactivates the AKT cell-survival pathway. Our study elucidates a previously unknown regulatory link between cell-death execution and cell-survival signaling.

Given the critical roles of the AKT kinases in cell growth, survival and metabolism, the activities of AKT kinases are tightly regulated at several different levels[9,14]. Association of AKT with PIP_3 generated by PI3K at the plasma membrane is the critical first step. This is followed by sequential phosphorylation of AKT by PDK1 and mTORC2, leading to full activation of AKT. At each step, negative regulators are in place to fine-tune the level of AKT activation. The PTEN phosphatase converts PIP_3 back to PIP_2, reducing or blocking AKT activation[49,50]. Dephosphorylation of AKT by phosphatases, including protein phosphatase 2A and phosphatase PHLPP, also reduces or blocks AKT activation[51–54]. In this study, we report a new mechanism that could rapidly

© 2014 Nature America, Inc. All rights reserved.

shut down AKT at the level of PIP_3 binding and plasma-membrane recruitment, through proteolytic activation of a PH-containing protein to generate a competing PI-binding activity. Given the presence of hundreds of PH-domain proteins with unknown functions in eukaryotes[41], this could be a general and conserved mechanism for regulating membrane-associated cell signaling or activity. There are several potential human CNT-1 homologs, ACAP1, ACAP2 and ACAP3, but none has been reported to have a role in apoptosis. It will be interesting to investigate whether these ACAP proteins might act like CNT-1 to inhibit AKT survival signaling in humans.

AKT kinases and PI3K are required for the IIS pathway in *C. elegans*. Inactivation of these genes increases life span and stress resistance[32,33]. Interestingly, loss of *cnt-1* does not affect these two processes (**Supplementary Fig. 8**), thus indicating that CNT-1 is an apoptosis-specific inhibitor of the PI3K-AKT pathway. AKT is a major drug target in treating cancer; however, clinical development of AKT inhibitors has been restricted by AKT's involvement in multiple important cellular events, which inevitably will lead to numerous on-target or off-target side effects[9,14,55]. Targeted inactivation of AKT in cancer cells to induce apoptosis through a CNT-1–like mechanism could present a new therapeutic strategy when combined with other anticancer therapies.

METHODS

Methods and any associated references are available in the online version of the paper.

Note: Any Supplementary Information and Source Data files are available in the online version of the paper.

ACKNOWLEDGMENTS

We thank B. Derry (Hospital for Sick Children) for anti–AKT-1 antibodies, M. Han (University of Colorado) for some RNAi clones, Y. Kohara (Japan National Institute of Genetics) for *akt-1* cDNA, M. Valencia and Y. Shi for making some of the constructs, S. Mitani (Tokyo Women's Medical University) and G. Ruvkun (Massachusetts General Hospital) for strains, R.R. Skeen-Gaar for assistance in generating transgenic strains and B.L. Harry, T. Blumenthal, B. Olwin, and J.M. Espinosa for comments on the manuscript. Some of the worm strains used in this study were kindly provided by the *Caenorhabditis* Genetics Center, which is funded by the US National Institutes of Health. This work was supported by US National Institutes of Health (grants R01 GM59083, R01 GM79097 and R01 GM088241 to D.X.).

AUTHOR CONTRIBUTIONS

A.N. and D.X. conceived the research and designed experiments. A.N. carried out and analyzed experiments. K.D.S. assisted in some experiments. A.N. and D.X. wrote the paper.

COMPETING FINANCIAL INTERESTS

The authors declare no competing financial interests.

Reprints and permissions information is available online at http://www.nature.com/reprints/index.html.

1. Steller, H. Mechanisms and genes of cellular suicide. *Science* **267**, 1445–1449 (1995).
2. Crawford, E.D. & Wells, J.A. Caspase substrates and cellular remodeling. *Annu. Rev. Biochem.* **80**, 1055–1087 (2011).
3. Rudel, T. & Bokoch, G.M. Membrane and morphological changes in apoptotic cells regulated by caspase-mediated activation of PAK2. *Science* **276**, 1571–1574 (1997).
4. Metzstein, M.M., Stanfield, G.M. & Horvitz, H.R. Genetics of programmed cell death in *C. elegans*: past, present and future. *Trends Genet.* **14**, 410–416 (1998).
5. Nakagawa, A., Shi, Y., Kage-Nakadai, E., Mitani, S. & Xue, D. Caspase-dependent conversion of Dicer ribonuclease into a death-promoting deoxyribonuclease. *Science* **328**, 327–334 (2010).
6. Breckenridge, D.G. *et al. Caenorhabditis elegans drp-1* and *fis-2* regulate distinct cell-death execution pathways downstream of *ced-3* and independent of *ced-9*. *Mol. Cell* **31**, 586–597 (2008).
7. Chen, Y.Z., Mapes, J., Lee, E.S., Skeen-Gaar, R.R. & Xue, D. Caspase-mediated activation of *Caenorhabditis elegans* CED-8 promotes apoptosis and phosphatidylserine externalization. *Nat. Commun.* **4**, 2726 (2013).
8. Cully, M., You, H., Levine, A.J. & Mak, T.W. Beyond PTEN mutations: the PI3K pathway as an integrator of multiple inputs during tumorigenesis. *Nat. Rev. Cancer* **6**, 184–192 (2006).
9. Luo, J., Manning, B.D. & Cantley, L.C. Targeting the PI3K-Akt pathway in human cancer: rationale and promise. *Cancer Cell* **4**, 257–262 (2003).
10. Staal, S.P., Hartley, J.W. & Rowe, W.P. Isolation of transforming murine leukemia viruses from mice with a high incidence of spontaneous lymphoma. *Proc. Natl. Acad. Sci. USA* **74**, 3065–3067 (1977).
11. Li, J. *et al.* PTEN, a putative protein tyrosine phosphatase gene mutated in human brain, breast, and prostate cancer. *Science* **275**, 1943–1947 (1997).
12. Vivanco, I. & Sawyers, C.L. The phosphatidylinositol 3-Kinase–AKT pathway in human cancer. *Nat. Rev. Cancer* **2**, 489–501 (2002).
13. Cho, H. *et al.* Insulin resistance and a diabetes mellitus-like syndrome in mice lacking the protein kinase Akt2 (PKBβ). *Science* **292**, 1728–1731 (2001).
14. Hers, I., Vincent, E.E. & Tavare, J.M. Akt signalling in health and disease. *Cell. Signal.* **23**, 1515–1527 (2011).
15. Finch, C.E. & Ruvkun, G. The genetics of aging. *Annu. Rev. Genomics Hum. Genet.* **2**, 435–462 (2001).
16. Kenyon, C. The plasticity of aging: insights from long-lived mutants. *Cell* **120**, 449–460 (2005).
17. Wolff, S. & Dillin, A. The trifecta of aging in *Caenorhabditis elegans*. *Exp. Gerontol.* **41**, 894–903 (2006).
18. Kimura, K.D., Tissenbaum, H.A., Liu, Y. & Ruvkun, G. *daf-2*, an insulin receptor-like gene that regulates longevity and diapause in *Caenorhabditis elegans*. *Science* **277**, 942–946 (1997).
19. Morris, J.Z., Tissenbaum, H.A. & Ruvkun, G. A phosphatidylinositol-3-OH kinase family member regulating longevity and diapause in *Caenorhabditis elegans*. *Nature* **382**, 536–539 (1996).
20. Wolkow, C.A., Munoz, M.J., Riddle, D.L. & Ruvkun, G. Insulin receptor substrate and p55 orthologous adaptor proteins function in the *Caenorhabditis elegans daf-2*/insulin-like signaling pathway. *J. Biol. Chem.* **277**, 49591–49597 (2002).
21. Paradis, S., Ailion, M., Toker, A., Thomas, J.H. & Ruvkun, G.A. PDK1 homolog is necessary and sufficient to transduce AGE-1 PI3 kinase signals that regulate diapause in *Caenorhabditis elegans*. *Genes Dev.* **13**, 1438–1452 (1999).
22. Paradis, S. & Ruvkun, G. *Caenorhabditis elegans* Akt/PKB transduces insulin receptor-like signals from AGE-1 PI3 kinase to the DAF-16 transcription factor. *Genes Dev.* **12**, 2488–2498 (1998).
23. Hertweck, M., Gobel, C. & Baumeister, R. *C. elegans* SGK-1 is the critical component in the Akt/PKB kinase complex to control stress response and life span. *Dev. Cell* **6**, 577–588 (2004).
24. Lin, K., Dorman, J.B., Rodan, A. & Kenyon, C. *daf-16*: an HNF-3/forkhead family member that can function to double the life-span of *Caenorhabditis elegans*. *Science* **278**, 1319–1322 (1997).
25. Ogg, S. *et al.* The Fork head transcription factor DAF-16 transduces insulin-like metabolic and longevity signals in *C. elegans*. *Nature* **389**, 994–999 (1997).
26. Lee, R.Y., Hench, J. & Ruvkun, G. Regulation of *C. elegans* DAF-16 and its human ortholog FKHRL1 by the *daf-2* insulin-like signaling pathway. *Curr. Biol.* **11**, 1950–1957 (2001).
27. Lin, K., Hsin, H., Libina, N. & Kenyon, C. Regulation of the *Caenorhabditis elegans* longevity protein DAF-16 by insulin/IGF-1 and germline signaling. *Nat. Genet.* **28**, 139–145 (2001).
28. Gil, E.B., Malone Link, E., Liu, L.X., Johnson, C.D. & Lees, J.A. Regulation of the insulin-like developmental pathway of *Caenorhabditis elegans* by a homolog of the PTEN tumor suppressor gene. *Proc. Natl. Acad. Sci. USA* **96**, 2925–2930 (1999).
29. Mihaylova, V.T., Borland, C.Z., Manjarrez, L., Stern, M.J. & Sun, H. The PTEN tumor suppressor homolog in *Caenorhabditis elegans* regulates longevity and dauer formation in an insulin receptor-like signaling pathway. *Proc. Natl. Acad. Sci. USA* **96**, 7427–7432 (1999).
30. Ogg, S. & Ruvkun, G. The *C. elegans* PTEN homolog, DAF-18, acts in the insulin receptor-like metabolic signaling pathway. *Mol. Cell* **2**, 887–893 (1998).
31. Rouault, J.P. *et al.* Regulation of dauer larva development in *Caenorhabditis elegans* by *daf-18*, a homologue of the tumour suppressor PTEN. *Curr. Biol.* **9**, 329–332 (1999).
32. Dorman, J.B., Albinder, B., Shroyer, T. & Kenyon, C. The *age-1* and *daf-2* genes function in a common pathway to control the lifespan of *Caenorhabditis elegans*. *Genetics* **141**, 1399–1406 (1995).
33. Larsen, P.L., Albert, P.S. & Riddle, D.L. Genes that regulate both development and longevity in *Caenorhabditis elegans*. *Genetics* **139**, 1567–1583 (1995).
34. Quevedo, C., Kaplan, D.R. & Derry, W.B. AKT-1 regulates DNA-damage-induced germline apoptosis in *C. elegans*. *Curr. Biol.* **17**, 286–292 (2007).
35. Parrish, J. *et al.* Mitochondrial endonuclease G is important for apoptosis in *C. elegans*. *Nature* **412**, 90–94 (2001).
36. Parrish, J.Z. & Xue, D. Functional genomic analysis of apoptotic DNA degradation in *C. elegans*. *Mol. Cell* **11**, 987–996 (2003).
37. Stanfield, G.M. & Horvitz, H.R. The *ced-8* gene controls the timing of programmed cell deaths in *C. elegans*. *Mol. Cell* **5**, 423–433 (2000).

© 2014 Nature America, Inc. All rights reserved.

38. Kokel, D., Li, Y., Qin, J. & Xue, D. The nongenotoxic carcinogens naphthalene and *para*-dichlorobenzene suppress apoptosis in *Caenorhabditis elegans*. *Nat. Chem. Biol.* **2**, 338–345 (2006).
39. Conradt, B. & Horvitz, H.R. The *C. elegans* protein EGL-1 is required for programmed cell death and interacts with the Bcl-2-like protein CED-9. *Cell* **93**, 519–529 (1998).
40. Xue, D., Shaham, S. & Horvitz, H.R. The *Caenorhabditis elegans* cell-death protein CED-3 is a cysteine protease with substrate specificities similar to those of the human CPP32 protease. *Genes Dev.* **10**, 1073–1083 (1996).
41. Park, W.S. *et al.* Comprehensive identification of PIP3-regulated PH domains from *C. elegans* to *H. sapiens* by model prediction and live imaging. *Mol. Cell* **30**, 381–392 (2008).
42. Tullet, J.M. *et al.* Direct inhibition of the longevity-promoting factor SKN-1 by insulin-like signaling in *C. elegans*. *Cell* **132**, 1025–1038 (2008).
43. Datta, S.R., Brunet, A. & Greenberg, M.E. Cellular survival: a play in three Akts. *Genes Dev.* **13**, 2905–2927 (1999).
44. Isakoff, S.J. *et al.* Identification and analysis of PH domain-containing targets of phosphatidylinositol 3-kinase using a novel *in vivo* assay in yeast. *EMBO J.* **17**, 5374–5387 (1998).
45. Parent, C.A., Blacklock, B.J., Froehlich, W.M., Murphy, D.B. & Devreotes, P.N. G protein signaling events are activated at the leading edge of chemotactic cells. *Cell* **95**, 81–91 (1998).
46. Meili, R. *et al.* Chemoattractant-mediated transient activation and membrane localization of Akt/PKB is required for efficient chemotaxis to cAMP in *Dictyostelium*. *EMBO J.* **18**, 2092–2105 (1999).
47. Servant, G. *et al.* Polarization of chemoattractant receptor signaling during neutrophil chemotaxis. *Science* **287**, 1037–1040 (2000).
48. Fayard, E., Tintignac, L.A., Baudry, A. & Hemmings, B.A. Protein kinase B/Akt at a glance. *J. Cell Sci.* **118**, 5675–5678 (2005).
49. Stambolic, V. *et al.* Negative regulation of PKB/Akt-dependent cell survival by the tumor suppressor PTEN. *Cell* **95**, 29–39 (1998).
50. Wu, X., Senechal, K., Neshat, M.S., Whang, Y.E. & Sawyers, C.L. The PTEN/MMAC1 tumor suppressor phosphatase functions as a negative regulator of the phosphoinositide 3-kinase/Akt pathway. *Proc. Natl. Acad. Sci. USA* **95**, 15587–15591 (1998).
51. Kuo, Y.C. *et al.* Regulation of phosphorylation of Thr-308 of Akt, cell proliferation, and survival by the B55α regulatory subunit targeting of the protein phosphatase 2A holoenzyme to Akt. *J. Biol. Chem.* **283**, 1882–1892 (2008).
52. Padmanabhan, S. *et al.* A PP2A regulatory subunit regulates *C. elegans* insulin/IGF-1 signaling by modulating AKT-1 phosphorylation. *Cell* **136**, 939–951 (2009).
53. Gao, T., Furnari, F. & Newton, A.C. PHLPP: a phosphatase that directly dephosphorylates Akt, promotes apoptosis, and suppresses tumor growth. *Mol. Cell* **18**, 13–24 (2005).
54. Brognard, J., Sierecki, E., Gao, T. & Newton, A.C. PHLPP and a second isoform, PHLPP2, differentially attenuate the amplitude of Akt signaling by regulating distinct Akt isoforms. *Mol. Cell* **25**, 917–931 (2007).
55. Cheng, G.Z. *et al.* Advances of AKT pathway in human oncogenesis and as a target for anti-cancer drug discovery. *Curr. Cancer Drug Targets* **8**, 2–6 (2008).

© 2014 Nature America, Inc. All rights reserved.
npg

ONLINE METHODS

Strains and culture conditions. *C. elegans* strains were maintained with standard procedures[56]. The following alleles were used in the genetic analyses. For LGI: *daf-16(mu86)*, *ced-1(e1735)*, *smIs13* and *smIs111*. For LGII: *dpy-10(e128)*, *age-1(mg44)*, *cnt-1(tm2313)*, *cps-2*(*sm8*) and *rol-1(e91)*. For LGIII: *daf-2(e1370)*, *ced-4(n1162*, *n2273)* and *smIs82*. For LGIV: *daf-18(e1375)*, *ced-3(n717*, *n2438)* and *dpy-4(e1166)*. For LGV: *akt-1(mg144gf*, *tm399)* and *him-5(e1490)*; LGX, *akt-2(tm1075)* and *sgk-1(ok538)*.

Isolation of the *cps-2*(*sm8*) mutation. Ethyl methane sulfonate (EMS) mutagenesis was performed on animals carrying an integrated transgene (*smIs1*) containing both $P_{mec\text{-}7}$acCED-3 and $P_{mec\text{-}3}$GFP[35]. $P_{mec\text{-}7}$acCED-3 drives acCED-3 expression in six mechanosensory neurons and also drives the ectopic death of these nonessential neurons, which were also labeled by GFP ($P_{mec\text{-}3}$GFP). Progeny of the mutagenized animals were screened for mutants with increased survival of the fluorescent mechanosensory neurons. From a screen of 3,000 mutagenized haploid genomes, we isolated several recessive mutations, including *sm8*, which defined a new gene, *cps-2* (CED-3 protease suppressor) on linkage group (LG) II. For the complementation-test result shown in **Figure 1a**, the complete genotype of *cps-2*(*sm8*)*/cnt-1(tm2313)* is *smIs13/+; cps-2*(*sm8*)*/cnt-1(tm2313); him-5(e1490)/+*. *smIs13* is an integrated line of $P_{sur\text{-}5}$SUR-5::GFP.

Quantification of cell corpses and extra cells. The number of cell corpses in living embryos and the number of extra cells in the anterior pharynxes of L4 larvae were scored with Nomarski optics as described previously[35].

CNT-1 antibody. Amino acids 1–298 of CNT-1b (tCNT-1b) fused with glutathione S-transferase (GST) were expressed in *Escherichia coli* strain BL21(DE3) and affinity purified from the soluble fraction of the bacterial lysate with glutathione Sepharose 4B beads (GE Healthcare). Rats were immunized with purified GST–tCNT-1b proteins (Spring Valley Laboratories). CNT-1 antibodies were affinity purified (Spring Valley Laboratories) from terminal bleeds with purified GST–tCNT-1a proteins as described previously[57].

Immunoblotting analysis. *C. elegans* embryos were harvested with M9, centrifuged at 500*g* to remove bacteria, and then sonicated in PBS buffer. After centrifugation at 25,400*g* to remove debris, 2× SDS loading buffer was added, and samples were heated at 95 °C for 3 min. The samples were resolved with 15% SDS-PAGE and transferred to PVDF membrane (Millipore). The membrane was first blocked with 5% nonfat dry milk in PBS-T (PBS plus 0.1% Tween 20) and washed two times with PBS-T for 5 min each. The membrane was then incubated with affinity-purified anti–CNT-1 antibody in 1:1,000 dilution for 1 h at room temperature and washed three times with PBS-T for 5 min each. It was then incubated with HRP-conjugated goat anti-rat IgG antibody (Jackson Immunoresearch, cat. no. 112-035-003; validation provided on the manufacturer's website) at 1:2,000 dilution for 1 h at room temperature, washed three times with PBS-T, and detected with enhanced chemiluminescent substrate (Pierce). For α-tubulin immunoblotting, anti–α-tubulin antibody (Developmental Studies Hybridoma Bank, cat. no. AA4.3; validation provided on the manufacturer's website) was used at 1:5,000 dilution, and HRP-conjugated goat anti-mouse IgG antibody (Jackson Immunoresearch, cat. no. 115-035-003; validation provided on the manufacturer's website) was used at 1:3,000 dilution. For anti-GST and anti-His_6 immunoblotting, a mouse anti-GST antibody (Santa Cruz Laboratory, cat. no. sc-138; validation provided on the manufacturer's website) or a rabbit anti-His_6 antibody (Santa Cruz Laboratory, cat. no. sc-803; validation provided on the manufacturer's website) was used at 1:2,000 dilution with an HRP-conjugated goat anti-mouse IgG antibody or an HRP-conjugated goat anti-rabbit IgG antibody (Jackson Immunoresearch, cat. no. 111-035-003; validation provided on the manufacturer's website) at 1:3,000 dilution. For anti–AKT-1 immunoblotting, an affinity-purified goat anti–AKT-1 antibody (Bethyl Laboratories)[58] was used at 1:10,000 dilution with an HRP-conjugated donkey anti-goat IgG antibody (Jackson Immunoresearch, cat. no. 705-035-003; validation provided on the manufacturer's website) at 1:10,000 dilution.

Heat-shock experiments. The heat-shock experiments were carried out as described previously[5].

CED-3–cleavage assay. CED-3 protease assays were done as described previously[40]. Briefly, proteins of interest were synthesized and labeled with ^{35}S-methionine with TNT Transcription and Translation coupled system (Promega) and incubated with or without 5 ng of purified CED-3 at 30 °C for 1 h. The reactions were then resolved by 15% SDS-PAGE gel and subjected to autoradiography.

Lipid binding assay. Various CNT-1 proteins were synthesized and labeled with ^{35}S-methionine with the TNT system and incubated with or without purified CED-3 as described above. The membrane strip containing various lipids (Echelon Biosciences) was blocked in 3% fatty acid–free bovine serum albumin (Sigma) in PBS-T (PBS plus 0.01% Tween 20) for 1 h and washed three times with PBS-T. The membrane strip was then incubated with 2 µl of the reticulocyte lysate containing the protein of interest at 1:1,000 dilution in PBS-T for 1 h at room temperature. After being washed three times with PBS-T, the membrane strip was subjected to autoradiography. For the PIP_3 competition assay, AKT-1, AKT-2 and SGK-1 were synthesized and labeled with ^{35}S-methionine, whereas GST–CNT-1 was synthesized with unlabeled methionine. After GST–CNT-1 was pretreated with CED-3, the lysate containing ^{35}S-methionine–labeled AKT-1 (20 µl) and the lysate containing unlabeled GST–CNT-1 (2 µl) were added to the membrane strip in 2 ml of PBS-T at the same time.

Determination of *in vitro*–synthesized protein concentrations. The concentrations of GST–tCNT-1a and AKT-1–His_6 synthesized in rabbit reticulocyte lysate (also labeled by ^{35}S-methionine) were determined by the immunoblotting analysis comparing the signal intensity of these proteins with that of recombinant GST–tCNT-1a (12 µg/ml) or AKT-1–His_6 (20 µg/ml) purified from bacteria. Recombinant GST–tCNT-1a or AKT-1–His_6 purified from bacteria did not show any lipid binding activity, probably owing to misfolding of the proteins. Briefly, 5.1 µl of GST–tCNT-1a or 2.9 µl of AKT-1–His_6 synthesized in rabbit reticulocyte lysate (*RRL) or 1 pmol of GST–tCNT-1a or AKT-1–His_6 purified from bacteria were resolved by 15% SDS-PAGE and subjected to immunoblotting analysis with an anti-GST or an anti-His_6 antibody as described above. Because the amounts of two GST–tCNT-1a proteins are comparable, the concentration of GST–tCNT-1a from RRL is approximately 196 nM. Because the amounts of two AKT-1–His_6 proteins are also comparable, the concentration of AKT-1–His_6 from RRL is approximately 345 nM.

Transgenic worms. Transgenic animals were generated as described previously[59]. $P_{cnt\text{-}1}$CNT-1a::3×Flag or $P_{cnt\text{-}1(sm8)}$CNT-1a::3×Flag was injected into *cps-2*(*sm8*) animals at 20 µg/ml along with the pTG96 plasmid (at 20 µg/ml) as a co-injection marker. The pTG96 plasmid contains a *sur-5::gfp* translational fusion that is expressed in all somatic cells at most developmental stages[60]. $P_{dpy\text{-}30}$CNT-1a, $P_{dpy\text{-}30}$CNT-1b, $P_{dpy\text{-}30}$CNT-1a(D1E), $P_{dpy\text{-}30}$CNT-1b(D1E), $P_{dpy\text{-}30}$tCNT-1a, $P_{dpy\text{-}30}$tCNT-1b, $P_{dpy\text{-}30}$CNT-1 F2, $P_{dpy\text{-}30}$CNT-1 F3, $P_{dpy\text{-}30}$CNT-1a(K284A), and $P_{dpy\text{-}30}$tCNT-1a(K284A) were injected into *cnt-1(tm2313)* animals at 20 µg/ml along with the pTG96 plasmid (at 20 µg/ml). Transgenic arrays containing $P_{dpy\text{-}30}$tCNT-1a were then crossed into the *akt-1(mg144gf)*, *age-1(mg44)* or *daf-16(mu86)* mutant for further analyses. $P_{sur\text{-}5}$AKT-1-PH::GFP was injected into *daf-18(e1375)* animals at 20 µg/ml along with the pRF4 (at 20 µg/ml), a dominant *rol-6* construct. One of the transgenic arrays was then crossed into N2 animals and *smIs82; daf-18(e1375)* animals or injected with $P_{dpy\text{-}30}$tCNT-1a at 20 µg/ml along with $P_{sur\text{-}5}$mCherry (at 20 µg/ml) as the second transgenic marker to generate transgenic animals containing both $P_{dpy\text{-}30}$tCNT-1a and $P_{sur\text{-}5}$AKT-1-PH::GFP. $P_{dpy\text{-}30}$AKT-1, $P_{dpy\text{-}30}$AKT-1(K222M), $P_{dpy\text{-}30}$AKT-2, or $P_{dpy\text{-}30}$AKT-2(K209M) was injected into *akt-1(tm399)/nT1; akt-2(tm1075)* animals at 20 µg/ml along with the pTG96 plasmid (at 20 µg/ml).

Molecular biology. Full-length *cnt-1a* cDNA and *cnt-1b* cDNA were amplified with reverse-transcription PCR (RT-PCR) and then subcloned into the pET-41b vector via its SpeI and NotI sites to generate the pET-41b-CNT-1a and pET-41b-CNT-1b expression vector. For the various pET-41b-CNT-1–mutant expression vectors (pET-41b-CNT-1a(D1E), pET-41b-CNT-1a(D2E), pET-41b-CNT-1a(D3E), pET-41b-CNT-1b(D1E), pET-41b-CNT-1b(D2E), pET-41b-CNT-1b(D3E), and pET-41b-CNT-1a(K284A)), pET-41b-CNT-1a or pET-41b-CNT-1b was used as a DNA template to make the indicated amino acid substitutions with a QuikChange mutagenesis kit (Stratagene).

© 2014 Nature America, Inc. All rights reserved.

pET-41b-tCNT-1a and pET-41b-tCNT-1b were constructed by subcloning of a PCR fragment encoding amino acids 1–382 of CNT-1a and 1–298 of CNT-1b into pET-41b via SpeI and EcoRV sites. For P_{cnt-1}CNT-1a::3×Flag, a 1,944-bp SphI–NheI PCR fragment containing the *cnt-1* promoter was fused with a 2,640-bp NheI–SmaI PCR fragment containing the full-length *cnt-1a* cDNA, which was then subcloned into a modified pPD95.79 vector in which the *gfp* coding region was replaced with a 3× Flag sequence. For P_{dpy-30}CNT-1a and P_{dpy-30}CNT-1b, full-length *cnt-1a* and *cnt-1b* cDNAs were PCR amplified and subcloned into pS235, which contains the promoter of the *C. elegans dpy-30* gene, via SphI and XmaI sites. QuikChange mutagenesis was then performed to obtain P_{dpy-30}CNT-1a (D1E) and P_{dpy-30}CNT-1b(D1E). P_{dpy-30}tCNT-1a and P_{dpy-30}tCNT-1b were constructed by subcloning of a PCR fragment encoding amino acids 1–382 of CNT-1a and 1–298 of CNT-1b into pS235 via its NheI and XmaI sites. For P_{dpy-30}CNT-1a F2 and P_{dpy-30}CNT-1a F3, PCR fragments encoding amino acids 383–609 and 610–826 of CNT-1a were subcloned into pS235 via NheI and XmaI sites. P_{dpy-30}CNT-1a(K284A) and P_{dpy-30}tCNT-1a(K284A) were generated by QuikChange mutagenesis. For the pET-21b-AKT-1, pET-21b-AKT-2, and pET-21b-SGK-1, expression vectors, *akt-1*, *akt-2*, and *sgk-1* full-length cDNAs were PCR amplified and subcloned into pET-21b through its NheI and XhoI sites. For the P_{sur-5}AKT-1-PH::GFP expression vector, a PCR fragment encoding amino acids 1–180 of AKT-1 was subcloned into a modified pPD95.77 vector, which contains the promoter of the *sur*-5 gene. P_{dpy-30}AKT-1 and P_{dpy-30}AKT-2 were constructed by subcloning theAKT-1 or AKT-2 cDNA fragment into the pS235 vector via its NheI and SmaI sites. QuikChange mutagenesis was then performed to generate kinase-defective mutants of AKT-1 and AKT-2 that contained K222M and K209M substitutions.

Determination of protein expression levels in *C. elegans*. 200 wild-type N2 *C. elegans* embryos at 1.5-fold stage were collected in PBS buffer and sonicated before addition of 2× SDS buffer. The N2 embryonic lysate and 1 pmol of GST–CNT-1a or AKT-1–His_6 proteins purified from bacteria were resolved by SDS-PAGE and subsequently subjected to immunoblotting with an affinity-purified anti–CNT-1 antibody or anti–AKT-1 antibody as described above, respectively. To determine the expression level from the immunoblotting images, the signal intensity of a protein band was measured with ImageJ software, and the background intensity–subtracted value was used to determine the average expression level of the protein.

Immunostaining on *C. elegans* embryos. Mixed-stage *C. elegans* animals were harvested with M9, bleached with 12% NaOCl and 1.5 M NaOH, and centrifuged at 500*g* to remove bacteria and debris. Embryos were washed three times with ddH_2O, mounted on poly-L-lysine–coated slides, and frozen at –80 °C for 10 min. They were fixed with methanol for 15 min on ice and washed with PBS before being stained with anti–CNT-1 antibody at 1:500 dilution in PBS for 1 h. After the embryos were washed three times with PBS, they were stained with Alexa Fluor 488–conjugated anti-rat IgG antibody (Molecular Probes, cat. no. A-11006; validation provided on the manufacturer's website) at 1:1,000 dilution in PBS for 1 h. They were then washed three times with PBS and visualized with an Axioplan 2 Nomarski Microscope (Carl Zeiss MicroImaging).

RT-PCR. The primer sequences for *cnt-1* were 5′-CTCTGTGCCAAGAC TGGATGC-GGGC-3′ and 5′-CGTTGCCTGGGACGCGGCGGAC- 3′, and the primer sequences for *rpl-26* were 5′-ATGAAGGTCAATCCGTTCGT-3′ and 5′-AGGACACGTCCAGTG-TTTCC-3′.

Lifespan analysis and thermotolerance assay. For lifespan analysis, animals were grown at 20 °C until the L4 larval stage and then transferred to new plates (ten animals per plate) at 25 °C. Animals were scored every day subsequently and moved periodically to keep growth conditions mold free. Animals were scored as dead if they failed to respond to a gentle tap on the head and tail with a platinum wire[21]. For thermotolerance assay, animals were grown at 20 °C until the L4 larval stage and then transferred to new plates (ten animals per plate) at 33 °C. Animals were scored every 2 h for the first 24 h and subsequently scored every 12 h until 60 h. Animals were scored as dead if they failed to respond to a gentle tap on the head and tail with a platinum wire.

RNAi experiments. RNAi experiments were carried out with a bacteria-feeding protocol described previously[61].

56. Brenner, S. The genetics of *Caenorhabditis elegans*. *Genetics* **77**, 71–94 (1974).
57. Wang, X. *et al*. *C. elegans* mitochondrial factor WAH-1 promotes phosphatidylserine externalization in apoptotic cells through phospholipid scramblase SCRM-1. *Nat. Cell Biol.* **9**, 541–549 (2007).
58. Perrin, A.J. *et al*. Noncanonical control of *C. elegans* germline apoptosis by the insulin/IGF-1 and Ras/MAPK signaling pathways. *Cell Death Differ.* **20**, 97–107 (2013).
59. Mello, C.C., Kramer, J.M., Stinchcomb, D. & Ambros, V. Efficient gene transfer in *C.elegans*: extrachromosomal maintenance and integration of transforming sequences. *EMBO J.* **10**, 3959–3970 (1991).
60. Gu, T., Orita, S. & Han, M. *Caenorhabditis elegans* SUR-5, a novel but conserved protein, negatively regulates LET-60 Ras activity during vulval induction. *Mol. Cell. Biol.* **18**, 4556–4564 (1998).
61. Tabara, H. *et al*. The *rde-1* gene, RNA interference, and transposon silencing in *C. elegans*. *Cell* **99**, 123–132 (1999).

© 2014 Nature America, Inc. All rights reserved.

doi:10.1038/nsmb.2915

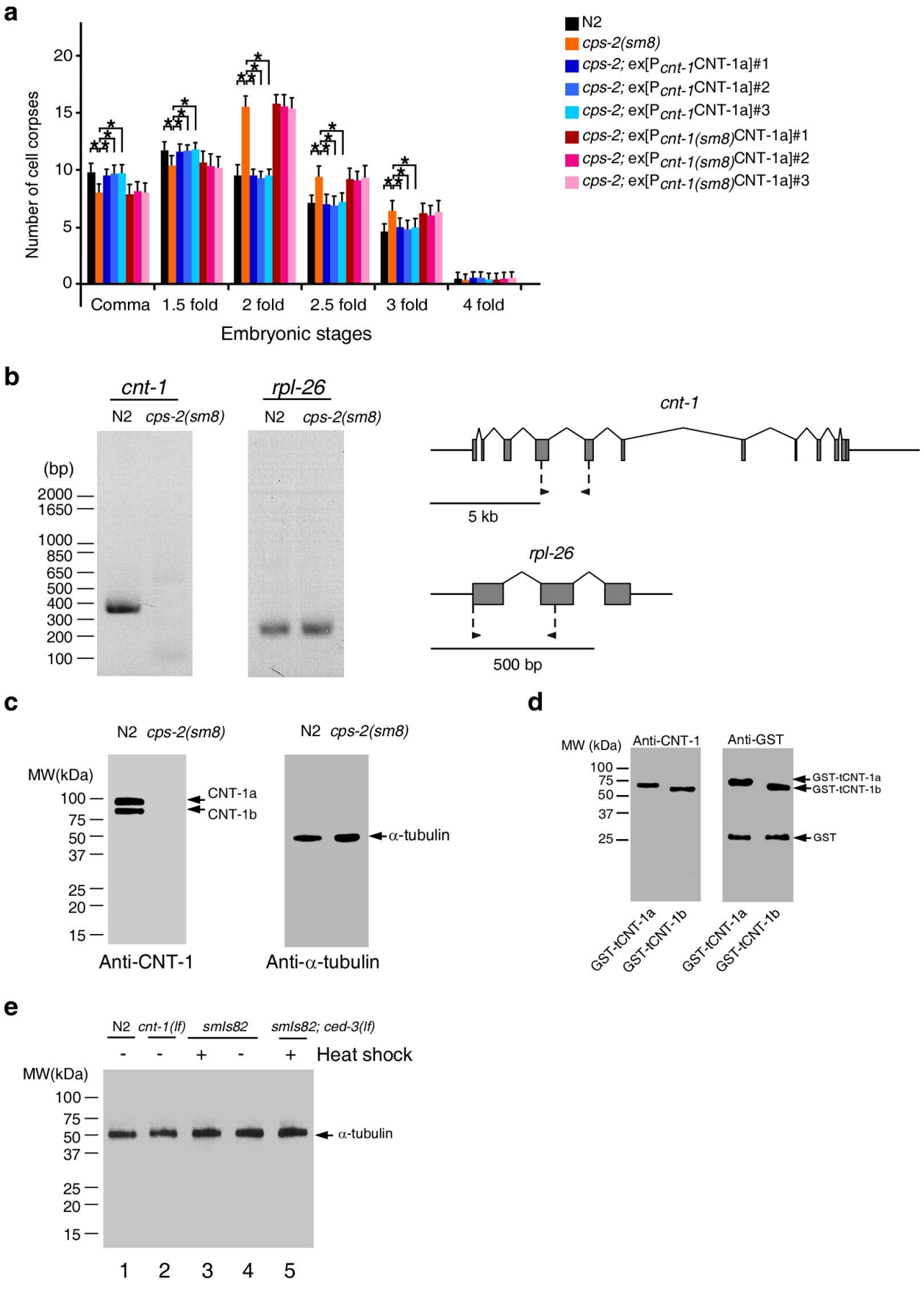
a
Number of cell corpses
Comma
1.5 fold
2 fold
2.5 fold
3 fold
4 fold
Embryonic stages
N2
cps-2(sm8)
cps-2; ex[Pcnt-1CNT-1a]#1
cps-2; ex[Pcnt-1CNT-1a]#2
cps-2; ex[Pcnt-1CNT-1a]#3
cps-2; ex[Pcnt-1(sm8)CNT-1a]#1
cps-2; ex[Pcnt-1(sm8)CNT-1a]#2
cps-2; ex[Pcnt-1(sm8)CNT-1a]#3
b
cnt-1
rpl-26
N2
cps-2(sm8)
(bp)
5 kb
500 bp
c
MW(kDa)
CNT-1a
CNT-1b
α-tubulin
Anti-CNT-1
Anti-α-tubulin
d
MW (kDa)
Anti-CNT-1
Anti-GST
GST-tCNT-1a
GST-tCNT-1b
GST
e
N2
cnt-1(lf)
smIs82
smIs82; ced-3(lf)
Heat shock
MW(kDa)
α-tubulin

Supplementary Figure 1

Analyses of the *cps-2(sm8)* mutant and anti–CNT-1 antibodies.

(**a**) Embryonic cell corpses were scored in the indicated animals. The y axis represents the average number of cell corpses and error bars are S.D. “ex” indicates an extrachromosomal array carrying the indicated construct. Statistical significance values were determined by two-way ANOVA, followed by Bonferroni comparison (n = 15 embryos). *, $P < 0.001$. All other points had $P > 0.05$. (**b**) RT-PCR analysis of N2 and *cps-2(sm8)* animals. Primer sets used for PCR are indicated with arrowheads in the cartoon. Left panel shows *cnt-1* and right panel shows *rpl-26* as a control. (**c**) Immunoblotting of N2 and *cps-2(sm8)* animals. Left panel is probed with anti-CNT-1 antibody and right panel is probed with anti-*∂*-tubulin antibody. (**d**) Immunoblotting of recombinant GST-tCNT-1a and GST-tCNT-1b. Left panel is probed with anti-CNT-1 antibody and right panel is probed with anti-GST antibody. (**e**) The uncropped image of *∂*-tubulin blot shown in **Fig. 2c**.

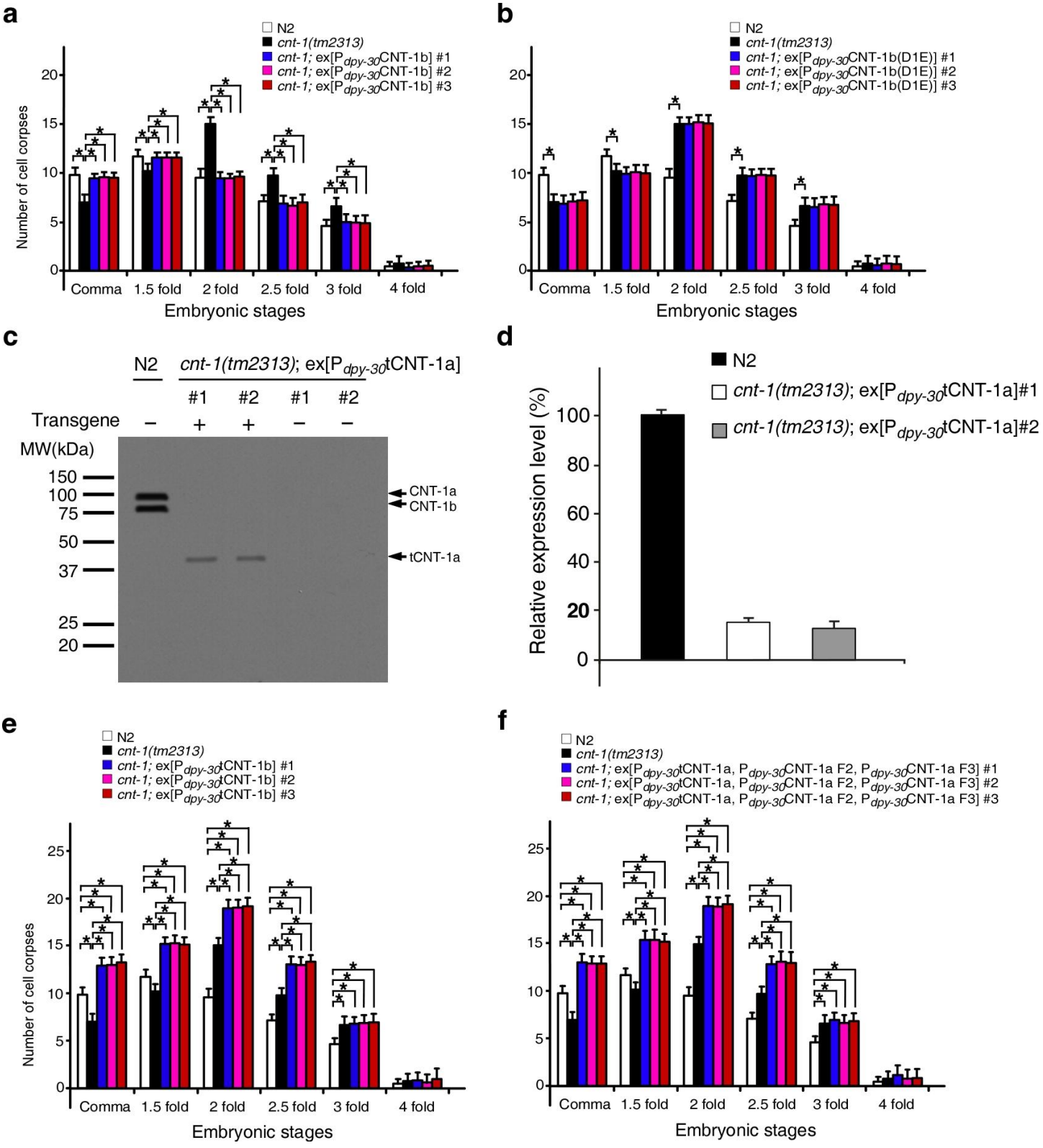

Supplementary Figure 2

CNT-1 cleavage by CED-3 is required for its proapoptotic function.

(**a,b** and **e,f**) Embryonic cell corpses were scored in animals with the indicate genotype. The y axis represents the average number of cell corpses and error bars represent S.D. Statistical significance values were determined by two-way ANOVA, followed by Bonferroni comparison (n = 15 embryos for each stage). *, $P < 0.001$. All other points had $P > 0.05$. (**c**) Ten L4 larvae with the indicated genotype were lysed in SDS loading buffer, resolved by 15% SDS-PAGE, and subjected to immunoblotting using an anti-CNT-1 antibody. (**d**) The relative CNT-1 protein expression levels determined from 3 independent experiments including **c**. The signal intensity of a protein band was measured using ImageJ and subtracted by the background intensity, the value of which was used to determine the average expression level of the protein. The data are presented as relative expression levels and S.D., with the CNT-1a expression level from N2 animals set as 100%.

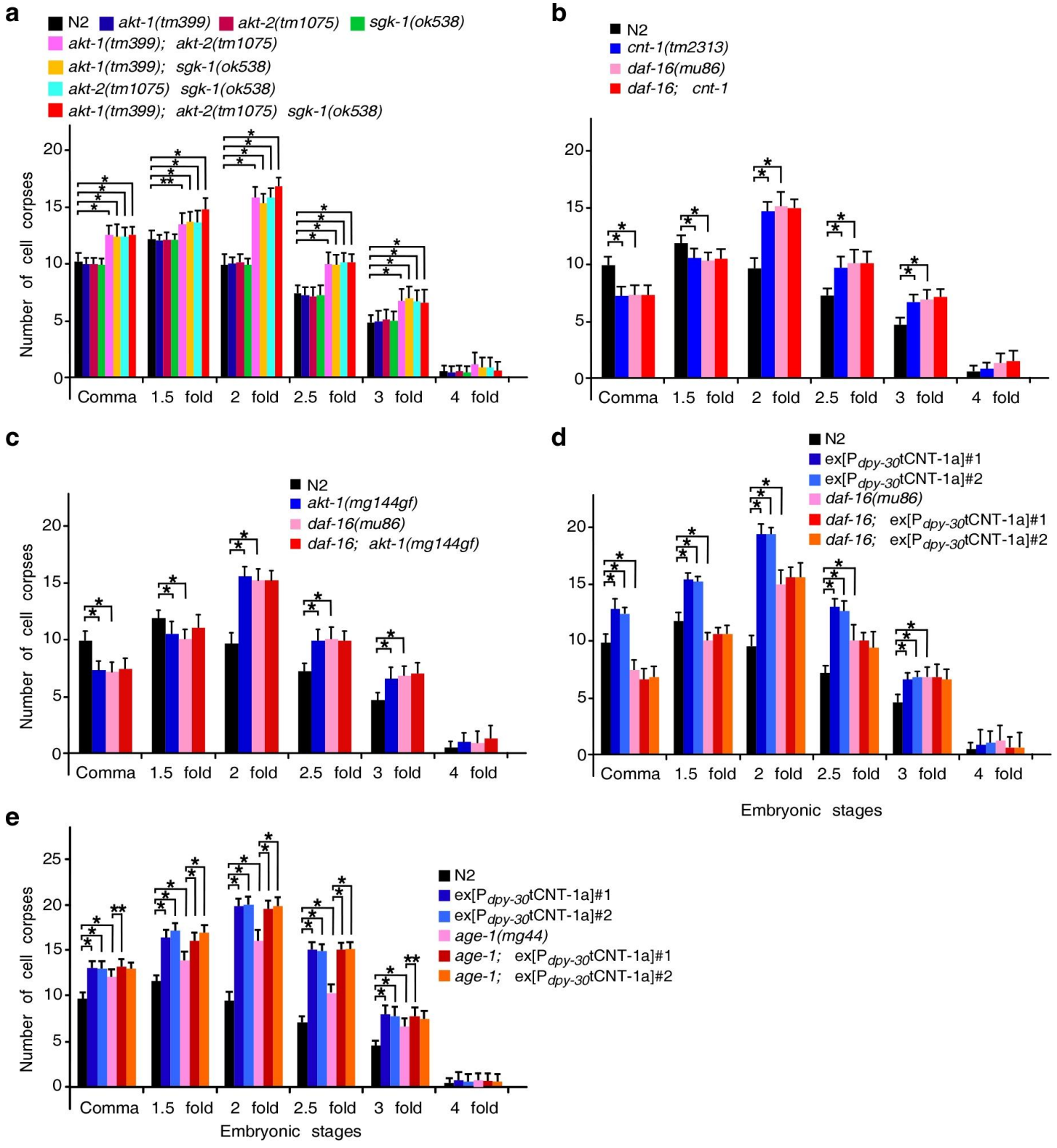

Supplementary Figure 3

Further analysis of the roles of AKT kinase genes, *age-1* and *daf-16* in *C. elegans* cell death.

Cell corpses were scored in the indicated strains. The y axis represents average number of cell corpses scored and error bars

represent S.D. Statistical significance values were determined by two-way ANOVA, followed by Bonferroni comparison (n = 15 embryos for each stage). *, $P < 0.001$; **, $P < 0.05$.

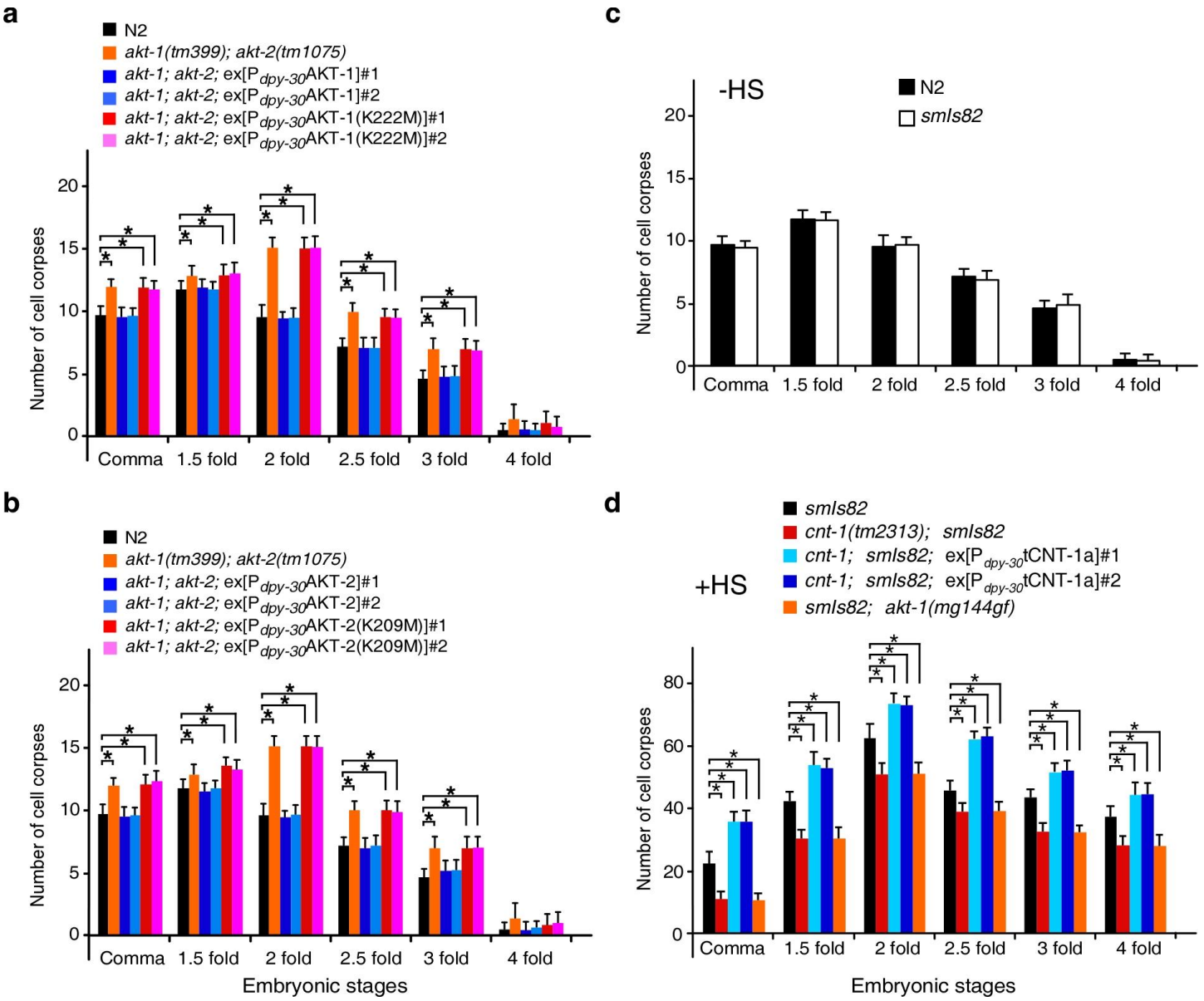

Supplementary Figure 4

Analyses of the importance of AKT-1 and AKT-2 kinase activities and CNT-1 in cell death in *C. elegans*.

Cell corpses were scored in the indicated strains. The y axis represents average number of cell corpses scored and error bars represent S.D. Statistical significance values were determined by two-way ANOVA, followed by Bonferroni comparison (n = 15 embryos for each stage). *, $P < 0.001$.

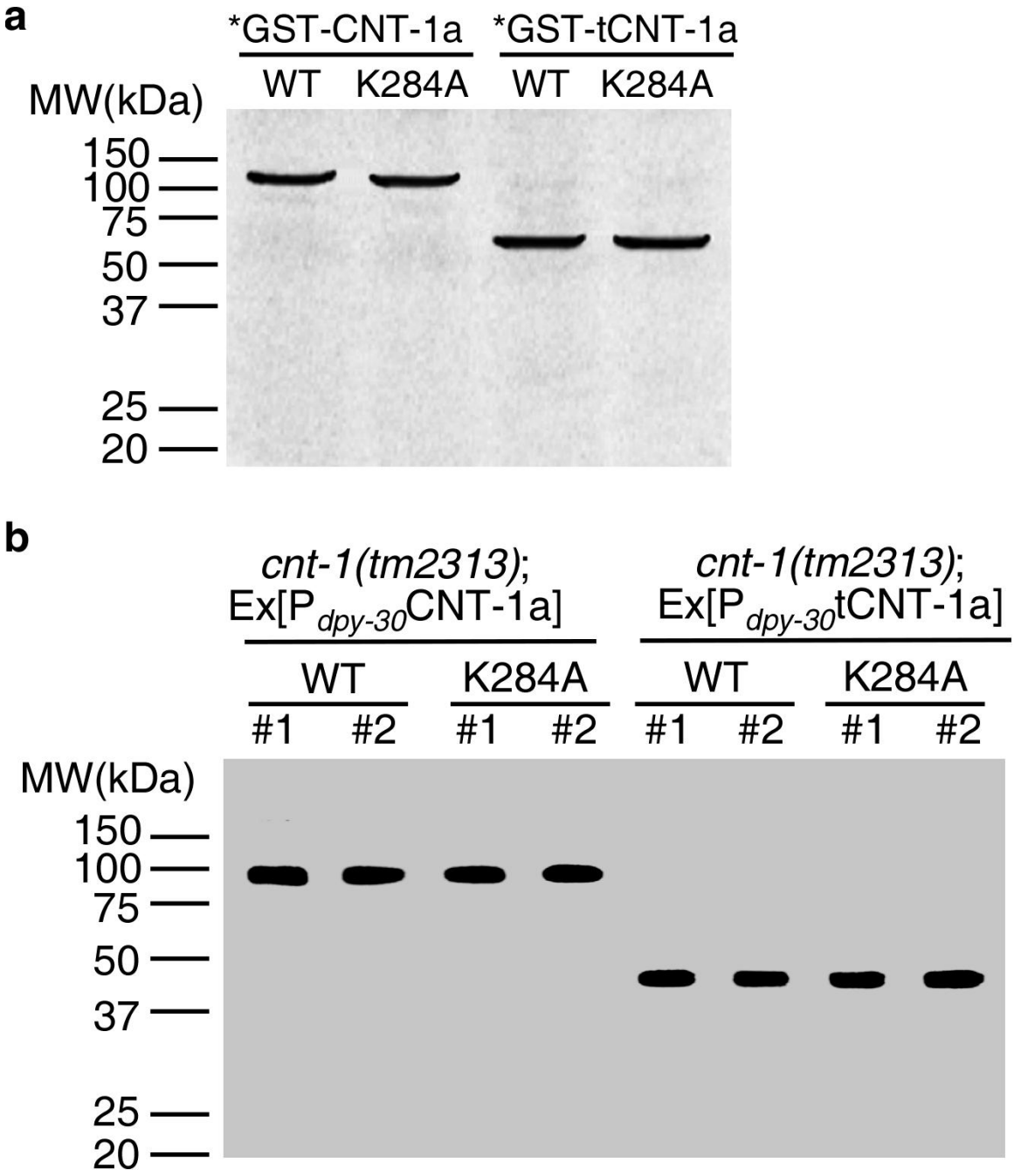

Supplementary Figure 5

Expression levels of CNT-1a(K284A) and tCNT-1a(K284A) are comparable to those of wild-type proteins both *in vitro* and *in vivo*.

(**a**) Autoradiogram of GST-CNT-1a, GST-CNT-1a(K284A), GST-tCNT-1a, and GST-tCNT-1a(K284A) synthesized in rabbit reticulocyte lysate and labeled with ^{35}S-Methionine (*). (**b**) Immunoblotting of worm lysates using an anti-CNT-1 antibody. Ten transgenic animals of the indicated genotype for each lane were subjected to immunoblotting.

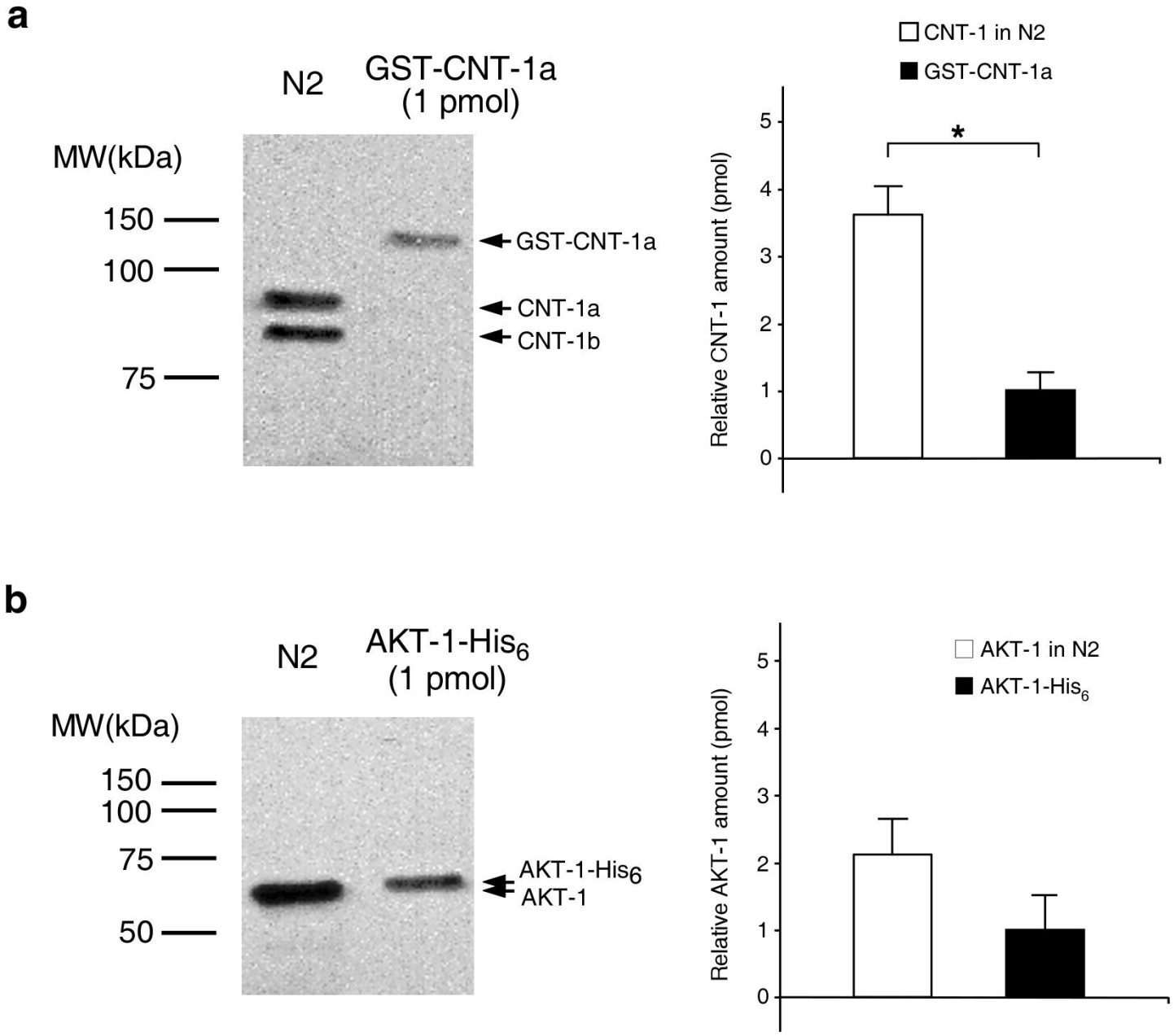

Supplementary Figure 6

The expression level of CNT-1 in *C. elegans* is higher than that of AKT-1.

(**a**) Left, immunoblotting of 100 N2 embryos at 1.5-fold stage and 1 pmol of GST-CNT-1a purified from bacteria using an anti-CNT-1 antibody. Right, quantification of the relative CNT-1 amount, which was determined from 3 independent experiments, including the one shown in the left panel, as described in **Supplementary Fig. 2d**. The data are presented as relative CNT-1 amount (CNT-1a+CNT-1b) and S.D. (**b**) Left, immunoblotting of 100 N2 embryos at 1.5-fold stage and 1 pmol of AKT-1-His_6 purified from bacteria using an anti-AKT-1 antibody. Right, the relative AKT-1 amount was determined as in **a**. Please see Online Methods for detail. Statistical significance values were determined by two-tailed Student's *t*-test (n = 3 independent experiments). *, $P < 0.001$ (**a**). $P > 0.05$ (**b**).

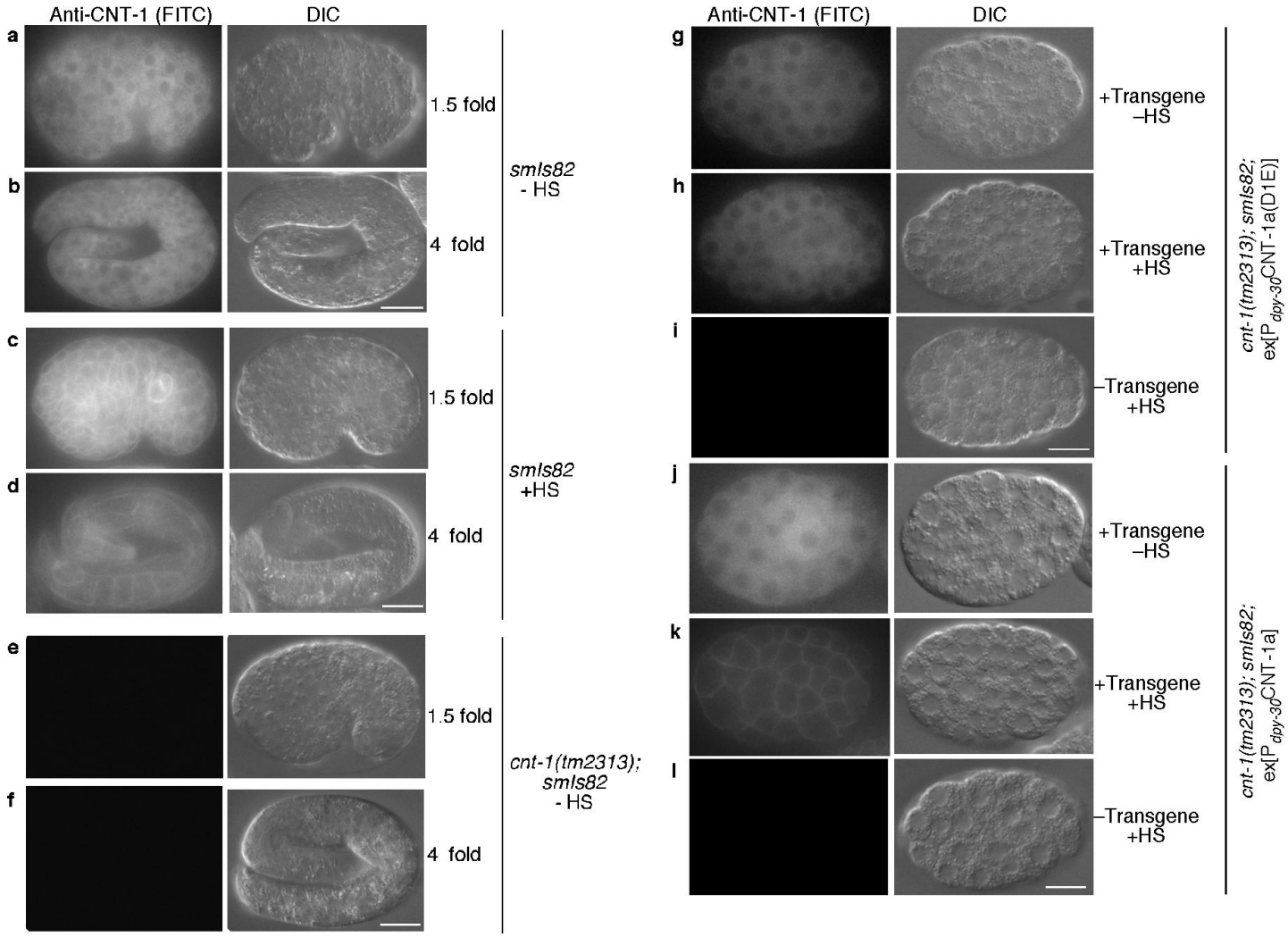

Supplementary Figure 7

Analyses of CNT-1 protein localization in various embryos.

(**a-f**) The CNT-1 protein is expressed in all cells during embryogenesis. Embryos with the indicated genotype and developmental stage were stained with an anti-CNT-1 antibody. FITC (left) and DIC (right) images are shown. (**g-l**) CED-3 uncleavable form of CNT-1a does not translocate to the plasma membrane after activation of CED-3 and apoptosis. Transgenic or non-transgenic embryos with the indicated genotype were stained with an anti-CNT-1 antibody. In all panels, -HS, no heat-shock treatment. +HS, with heat-shock treatment. Scale bars represent 10 mm.

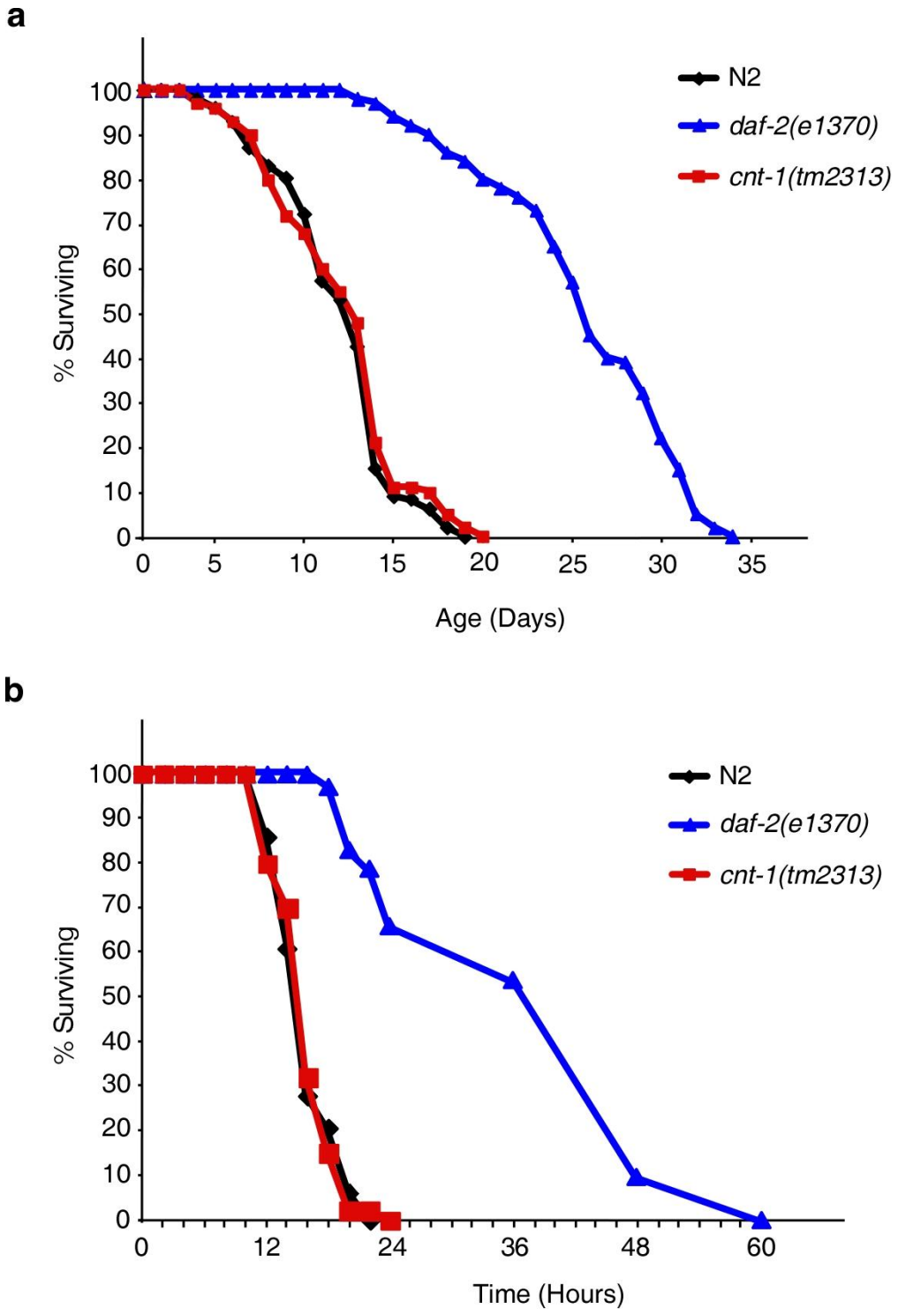

Supplementary Figure 8

The *cnt-1(tm2313)* deletion does not affect life span or thermotolerance.

Animals with the indicated genotype were subjected to either life span analysis (**a**) or heat stress resistance analysis (**b**) (see Online Methods).

Supplementary Note

Altered CNT-1 activity affects apoptosis induced by *smIs82*

We scored cell corpses in *smIs82* embryos to examine if loss of *cnt-1* is capable of suppressing cell death after the CED-3 caspase is globally activated. In the absence of the heat shock treatment, *smIs82* embryos showed a cell corpse profile similar to that of N2 embryos (**Supplementary Fig. 4c**). After the heat shock treatment, the numbers of cell corpses in *smIs82* embryos were dramatically increased (**Supplementary Fig. 4d**), indicating that many cells are induced to undergo apoptosis. We found that loss of *cnt-1* partially suppressed and expression of tCNT-1a enhanced ectopic cell death induced by *smIs82* (**Supplementary Fig. 4d**), providing further supporting evidence that *cnt-1* acts downstream of CED-3 to promote apoptosis. A similar partial suppression of cell death was accomplished by a gain-of-function *akt-1(mg144gf)* mutation (**Supplementary Fig. 4d**), confirming that *akt-1* can also inhibit cell death downstream of EGL-1 and CED-3.

Nature Structural and Molecular Biology: doi:10.1038/nsmb.2915

Supplementary Tables

Supplementary Table 1 RNAi treatment of *cnt-1* caused a delay-of-cell-death phenotype similar to that of the *cps-2(sm8)* mutant.

RNAi clone	**Cell death defect**
vector RNAi	–
tpi-1	–
Y17G7B.10	–
arrd-7	–
arrd-8	–
cnt-1	+
Y17G7B.17	–
Y17G7B.18	–
Y17G7B.19	–
Y43F11A.1	–

N2 animals were treated with RNAi and cell corpses in embryos were scored as described in METHODS. For each RNAi experiment, 15 embryos each at the comma, 1.5 fold, 2 fold, 2.5 fold, 3 fold, and 4 fold embryonic stages were scored. The candidate genes tested and corresponding RNAi results are summarized above. "+" indicates that the RNAi clone caused a delay-of-cell-death defect. "–" indicates that there was no obvious cell death defect.

Supplementary Table 2 Inactivation of *cnt-1* enhances suppression of cell death.

Genotype	No. of extra cells	Range of extra cells
N2	0.1 ± 0.1	0–1
cnt-1(tm2313)	0.1 ± 0.1	0–1
ced-3(n2438)	1.3 ± 0.3	0–3
cnt-1(tm2313); ced-3(n2438)	3.5 ± 0.3*	2–6
ced-4(n2273)	2.2 ± 0.4	0–5
cnt-1(tm2313); ced-4(n2273)	3.4 ± 0.4**	1–6

Extra cells were scored in the anterior pharynx of L4 hermaphrodites using Nomarski optics as described in METHODS. Data shown are mean ± s.e.m. Statistical significance values were determined by one-way ANOVA, followed by Tukey's test (n = 20 animals). * $P < 0.001$, compared with *ced-3(n2438)*. ** $P < 0.05$, compared with *ced-4(n2273)*.

Supplementary Table 3 Expression of tCNT-1 causes ectopic cell death.

Genotype	No. of missing cells	Range of missing cells
N2	0 ± 0	0
cnt-1(tm2313)	0 ± 0	0
cnt-1; ex[P_{dpy-30}tCNT-1a] #1	0.3 ± 0.1*	0–1
cnt-1; ex[P_{dpy-30}tCNT-1a] #2	0.35 ± 0.1*	0–1
cnt-1; ex[P_{dpy-30}tCNT-1a] #3	0.35 ± 0.1*	0–1
cnt-1; ex[P_{dpy-30}tCNT-1b] #1	0.3 ± 0.1*	0–1
cnt-1; ex[P_{dpy-30}tCNT-1b] #2	0.3 ± 0.1*	0–1
cnt-1; ex[P_{dpy-30}tCNT-1b] #3	0.35 ± 0.1*	0–1

Missing cells were scored in the anterior pharynx of L4 transgenic hermaphrodites using Nomarski optics. Data shown are mean ± s.e.m. Statistical significance values were determined by one-way ANOVA, followed by Tukey's test (n = 20 animals). *$P < 0.001$, compared with *cnt-1(tm2313)* animals.

Supplementary Table 4 Increased activity of *akt-1* and loss of *daf-18* both inhibit apoptosis.

Genotype	No. of extra cells	Range of extra cells
N2	0.1 ± 0.1	0–1
akt-1(mg144gf)	0.1 ± 0.1	0–1
ced-3(n2438)	1.3 ± 0.3	0–3
ced-3(n2438); akt-1(mg144gf)	3.4 ± 0.4*	1–6
daf-16(mu86)	0.1 ± 0.1	0–1
daf-16(mu86); ced-3(n2438)	3.5 ± 0.4*	1–6
daf-18(e1375)	0.1 ± 0.1	0–1
ced-3(n2438) dpy-4(e1166)	1.4 ± 0.3	0–3
daf-18(e1375) ced-3(n2438) dpy-4(e1166)	3.5 ± 0.3**	1–5

Extra cells were scored in the anterior pharynx of L4 hermaphrodites using Nomarski optics. Data shown are mean ± s.e.m. Statistical significance values were determined by one-way ANOVA, followed by Tukey's test ($n = 20$ animals). *$P < 0.001$; compared with *ced-3(n2438)*. ** $P < 0.001$; compared with *ced-3(n2438) dpy-4(e1166)*.

Supplementary Table 5 *cnt-1* acts downstream of *age-1* and upstream of *akt-1, akt-2* and *sgk-1* to promote apoptosis.

Genotype	No. of missing cells	Range of missing cells
N2	0 ± 0	0
cnt-1(tm2313)	0 ± 0	0
age-1(mg44)	0.35 ± 0.11*	0–1
age-1(mg44) cnt-1(tm2313)	0 ± 0	0
akt-1(tm399); akt-2(tm1975) sgk-1(ok538)	0.35 ± 0.11*	0–1
cnt-1(tm2313); akt-1(tm399); akt-2(tm1975) sgk-1(ok538)	0.40 ± 0.11**	0–1

Missing cells were scored in the anterior pharynx of L4 hermaphrodites using Nomarski optics. Data shown are mean ± s.e.m. Statistical significance values were determined by one-way ANOVA, followed by Tukey's test ($n = 20$ animals). *$P < 0.001$, compared with N2. **$P < 0.001$, compared with *cnt-1(tm2313)*.